

# Internal Waves and Tidal Conversion from a Finite Submarine Ridge

Blagoje Djordjevic

adviser: P.J. Morrison

Physics Department, University of Texas at Austin, 2012

## Abstract

The purpose of this study is to investigate how the shape of a submarine ridge on the ocean bottom affects the generation of internal tidal waves. Expanding upon previous studies of the knife edge, an infinitesimally thin ridge, we used perturbation theory to observe how a finite width affects the conversion rate, stream function and vorticity field generated. We departed from previous analytical studies by considering an asymmetric triangular ridge. The techniques used can be extended to different types of physical problems, both in ocean science and elsewhere.

# 1 Introduction

The ocean is a continuously stratified fluid that varies in pressure, density, and composition along the vertical, parallel to the force of gravity. In shallow waters, these variations are not very pronounced and the effects of stratification can be ignored. In the open ocean, at depths as great as several kilometers, stratification has clear consequences, such as the creation and propagation of internal waves. In the simplest case we see waves at the interface between fluids of very different densities, e.g. the air and water. Any disturbance occurring at this interface propagates as waves. The ocean, due to the constantly varying density gradient, effectively has a long boundary gradient across its entire depth, by which internal waves occur. Internal waves are studied for a variety of reasons, most notably because it appears that they account for the mixing of the ocean waters even at great depths. They also account for the dissipation of a considerable portion of the lunar tidal energy and in consequence to the gradual slowing down of Earth's Moon.

The most common drivers of internal waves are lunar tides in the deep ocean. The oscillatory flow of the water at the tidal frequency impinges on the ocean floor topography and causes the dissipation of energy by means of the radiation of internal gravity waves. In a density stratified fluid, which in the ocean is caused by variations in salinity and temperature, internal waves are not isotropic and their frequency is determined by the direction of propagation with respect to the vertical. The frequency of these waves satisfies the inequality  $\omega \leq N$ , where  $N$  is the buoyancy frequency or Brunt-Väisälä frequency. Another interesting feature of internal waves is that their phase and group velocities are perpendicular to one another.

Several approaches to defining and modelling internal waves have been attempted, both analytical and numerical. As early as 1969 Robinson [14] came up with an analytical solution for the knife edge (an infinitely thin barrier of a height much smaller than the ocean depth) that has served as the basis for several subsequent papers. In 1975 Bell [2] used the weak topography approximation (WTA) to get an estimation for the rate of tidal conversion, where the slope of topographical variations is smaller than the angle of propagation of internal waves and the height of the topography is much smaller than the ocean depth. Most subsequent studies of internal waves, especially in the past two decades, focused on numerical methods.

This thesis follows the analytical approach formulated by Robinson [14] and extended by Petrelis, Smith and Young [13], [7], [8]. This entails the formulation of an analytic expression for the stream function as a convolution of the Green's function, or 'vortex solution' as Robinson called it, and a source function defined at the surface of the ridge. The source function, which is not known a priori, represents the strength by which waves are generated or scattered on the surface of ocean's topography. The Green's function is

precisely determined for the case of buoyancy frequency independent of depth  $z$ . It is formulated as an approximation in the sense of the WKB method for slowly varying variables, i.e. the density stratification. For every particular topography with an established Green function and a known value of the stream function along the topography, one can treat the resulting equation as an integral equation for the source density function on that particular topography. In the case of the knife edge, the equation for the source function reduces to a well known form familiar from airfoil theory and can be solved exactly, as demonstrated by Smith and Young [8].

This study, following Pétrélis, analyzes a thin triangular ridge, as opposed to the knife edge. We employ perturbation theory and the aforementioned integral equation method. We hope to develop a model in which we can get an analytic solution for a more complicated system than the knife edge. Likewise, the fact that our ridge is not infinitely thin means that we can introduce asymmetries into the problem and examine how asymmetries affect the generation of tidal waves. This a factor not considered by Young or Pétrélis but examined by Echeverri and Peacock [3] numerically.

## 2 Background: Derivation of the Governing Equations

### 2.1 Vertical Density Stratification and Wave Motion

Internal waves are movements of local volume elements in a density stratified fluid where the restoring force is provided by the buoyancy pressure exerted by the surrounding fluid. Let us denote the density of the fluid element, which is conserved in this movement, as  $\rho_0(0)$ . In a stable, stratified fluid the density increases with depth. Let us imagine that the volume element is displaced downwards from its equilibrium position by a small amount  $\xi$ . The change in pressure experienced by the fluid element is  $dp = -\rho_0 g \xi$  while the variation of the surrounding fluid's density is  $d\rho = dp/c^2$ , where  $c$  is the speed of sound in the fluid. The element coming from above is lighter and is pushed upward by the surrounding, more dense fluid. A converse effect takes place when that element tries to move upwards. Then the buoyancy force acting on a displaced volume element introduces a force which provides a downwards acceleration, so that

$$g\Delta\rho = g[(\rho_0 + \rho_{0z}\xi) - (\rho_0 - \rho_0 g \xi / c^2)] - \rho_0 \xi_{tt}, \quad (1)$$

where  $\Delta\rho = \rho_{out} - \rho_{in} = 0$  under the assumption that the element density does not change. This equation can be rearranged as

$$\xi_{tt} + \xi \left( -\frac{g\rho_{0z}}{\rho_0} - \frac{g^2}{c^2} \right) = 0. \quad (2)$$

Equation (2), describing time variation of position of the element at  $\xi$ , is the equation for a simple harmonic oscillator with a solution of the form:  $Ae^{\pm iNt}$ , where

$$N(z) = \left( -\frac{g}{\rho_0} \frac{d\rho_0}{dz} - \frac{g^2}{c^2} \right)^{1/2} \approx \left( -\frac{g}{\rho_0} \frac{d\rho_0}{dz} \right)^{1/2} \quad (3)$$

is the frequency of oscillations. Since  $\frac{g^2}{c^2}$  is usually very small in comparison to  $\frac{g}{\rho_0} \frac{d\rho_0}{dz}$  it will be neglected here. The element oscillates about its equilibrium position at a natural frequency determined by the local density stratification and the fluid's compressibility. This frequency is known as the Brunt-Väisälä frequency or buoyancy frequency as noted earlier and is often used to characterize the degree of stratification in the ocean.

To reiterate, a good way to visualize the described mechanism is to imagine a barrel floating on the surface of the water. When someone pushes the barrel down into the water, the change in relative

buoyancy will cause the barrel to float up. However, the acquired velocity will make the barrel pass its equilibrium position and move up into the air. Subsequently gravity will pull it down and the process continues. The barrel will keep oscillating (at its buoyancy frequency) until the energy is dissipated fully into waves propagating outwards along the water surface. The same mechanism takes place in a density stratified fluid except that a density gradient exists throughout the fluid, not just at the boundary between the fluid and the air.

## 2.2 Equations of Motion

To describe the dynamics of internal waves in full we must consider a more detailed description of fluid motion. We can start with the Navier-Stokes equations, which for an incompressible fluid in two dimensions read:

$$\frac{1}{\rho} \frac{D\rho}{Dt} + \frac{\partial u}{\partial x} + \frac{\partial w}{\partial z} = 0 \quad (4)$$

$$\rho \frac{\partial u}{\partial t} + u \frac{\partial u}{\partial x} = -\frac{\partial p}{\partial x} \quad (5)$$

$$\rho \frac{\partial w}{\partial t} + w \frac{\partial w}{\partial z} = -\frac{\partial p}{\partial z} - \rho g \quad (6)$$

$$\frac{\partial \rho}{\partial t} + u \frac{\partial \rho}{\partial x} + w \frac{\partial \rho}{\partial z} = 0, \quad (7)$$

where  $\frac{D}{Dt}$ ,  $x$ ,  $z$ ,  $u$ ,  $w$ ,  $\rho$ , and  $p$  are the total time derivative, horizontal coordinate, vertical coordinate, horizontal velocity, vertical velocity, density and pressure, respectively. In the above equations we ignore the horizontal coordinate  $y$ , because for the most part we are concerned with waves propagating in one direction, the direction of the lunar tide. The equations above also do not account for the Coriolis force (the effects of the Earth's rotation), often represented by the Coriolis frequency  $f$ . Equation (4) is the continuity equation, (5) and (6) are the momentum conservation equations, and (7) is the mass conservation equation.

One solution of equations (4) to (7) is motionless, hydrostatic balance, that is  $\mathbf{u}_0 = 0$ ;  $-p_{0,z} - \rho_0(0)g = 0$ . If we presume that the internal waves cause only small departures of all variables from those established by hydrostatic equilibrium, each variable can be separated into a hydrostatic component and a

small perturbation signified by the subscript 0, that is:

$$\mathbf{u} = \mathbf{u}_0 + \mathbf{u}_1, \quad \mathbf{w} = \mathbf{w}_0 + \mathbf{w}_1, \quad p = p_0 + p_1, \quad \rho = \rho_0 + \rho_1. \quad (8)$$

Now we can consider a wave of small amplitude in an inviscid, non-diffusive fluid. Substituting these back into our equations we can linearize these equations by ignoring all non-linear terms. Taking into consideration that  $\frac{\partial \rho}{\partial x} = 0$  (since the density only varies in the  $z$ -direction), we get

$$\frac{\partial u_0}{\partial x} + \frac{\partial w_0}{\partial z} = 0 \quad (9)$$

$$\rho_0 \frac{\partial u_0}{\partial t} = - \frac{\partial p_0}{\partial x} \quad (10)$$

$$\rho_0 \frac{\partial w_0}{\partial t} = - \frac{\partial p_0}{\partial z} - \rho_0 g \quad (11)$$

$$\frac{\partial \rho_0}{\partial t} + w_0 \frac{\partial \rho_0}{\partial z} = 0. \quad (12)$$

The Boussinesq approximation is often applied to these equations, which entails further treating the coefficient  $\rho_0$  as constant in equations (10) and (11) and redefining the partial derivative  $\frac{\partial \rho_0}{\partial z}$  as  $\frac{\partial \rho}{\partial z}$ .

Equations (9) through (12) can be reformulated as a set of linear equations in matrix form:

$$\begin{aligned} \rho_0 \frac{\partial u_0}{\partial t} &+ & & + \frac{\partial p_0}{\partial x} & & = 0 \\ & & \rho_0 \frac{\partial w_0}{\partial t} & + \frac{\partial p_0}{\partial z} & + \rho_0 g & = 0 \\ & & & & & \frac{d\rho}{dt} w & + & + \frac{\partial \rho}{\partial t} & = 0 \\ \frac{\partial u_0}{\partial x} &+ \frac{\partial w_0}{\partial z} & & & & = 0 \end{aligned} \quad (13)$$

If we assume that there exists a simple harmonic solution of frequency  $\omega$ , and a wave vector with components  $k_x$  and  $k_y$ , i.e.

$$\begin{bmatrix} u_0 \\ w_0 \\ p_0 \\ \rho_0 \end{bmatrix} = e^{i(k_x x + k_y y - \omega t)} \begin{bmatrix} \tilde{u}_0 \\ \tilde{w}_0 \\ \tilde{p}_0 \\ \tilde{\rho}_0 \end{bmatrix} \quad (14)$$

the set of differential equations (9 - 12) is transformed into a set of linear equations in  $(\omega, k_x, k_z)$  with

unknown amplitudes  $u_0$ ,  $w_0, p_{10}$  and  $\rho_{10}$ :

$$\begin{bmatrix} -i\omega\rho_0 & 0 & ik_x & 0 \\ 0 & -i\omega\rho_0 & ik_y & g \\ 0 & \frac{d\rho_0}{dy} & 0 & -i\omega \\ ik_x & ik_y & 0 & 0 \end{bmatrix} \begin{bmatrix} \tilde{u}_0 \\ \tilde{w}_0 \\ \tilde{p}_0 \\ \tilde{\rho}_0 \end{bmatrix} = 0 \quad (15)$$

This set of equations has a non-trivial solution if the determinant of the matrix on the left is equal to zero.

The value of the determinant can be determined to be:

$$\begin{aligned} & -i\omega\rho_0 \begin{bmatrix} -i\omega & ik_y & g \\ \frac{d\rho_0}{dy} & 0 & -i\omega \\ ik_y & 0 & 0 \end{bmatrix} + ik_x \begin{bmatrix} 0 & -i\omega\rho_0 & g \\ 0 & \frac{d\rho_0}{dy} & -i\omega \\ ik_x & ik_y & 0 \end{bmatrix} \\ & = -i\omega(ik_y)(ik_y)(-i\omega) + (ik_x)(ik_x)((-i\omega\rho_0)(-i\omega) - g\frac{d\rho_0}{dy}) \\ & = \rho_0\omega^2k_y^2 - (-\rho_0\omega^2 - g\frac{d\rho_0}{dy})k_x^2 = 0 \end{aligned} \quad (16)$$

The last equality establishes the dispersion relation that relates the frequency  $\omega$  and the wave vector components  $k_y$  and  $k_x$ . From equation (16) we can deduce that the ratio of the vertical component,  $k_y$ , and the horizontal component,  $k_x$ , of the wave vector  $k$  describing the propagation of internal waves, is equal to

$$\frac{k_y}{k_x} = \tan(\alpha) = \left( \frac{-\omega^2 - \frac{g}{\rho_0} \frac{d\rho}{dy}}{\omega^2} \right)^{1/2} = \pm \left( \frac{N - \omega^2}{\omega^2} \right)^{1/2} \quad (17)$$

This itself is an interesting result, stating that all internal waves of frequency  $\omega$ , and given buoyancy frequency  $N$ , always propagate with the same angle with respect to the horizontal axis.

Equations (9 - 12) can be further simplified by eliminating some of the unknown variables. We can also drop index 0 from variables  $u_0$  and  $w_0$  and start calling them  $u$  and  $w$ , (the horizontal and vertical velocities). Let us reformulate the terms in the set of equations (15) in  $\omega$ -space as,

$$\frac{\partial u}{\partial x} + \frac{\partial w}{\partial z} = 0 \quad (18)$$

$$-i\omega u = -\frac{1}{\rho_0} \frac{\partial p}{\partial x} \quad (19)$$

$$-i\omega w = -\frac{1}{\rho_0}\left(\frac{\partial p}{\partial z} + \rho g\right) \quad (20)$$

$$-i\omega\rho_0 + w_0\frac{\partial\rho}{\partial z} \quad (21)$$

If we insert the value of  $\rho$  from the mass equation (21) into the  $z$ -component of the momentum equation (20) we obtain the relation

$$\rho_0(N^2 - \omega^2)w_0 = i\omega\frac{\partial p}{\partial z} \quad (22)$$

The  $x$  and  $y$  components of velocity may further be rewritten as,

$$u = \frac{-i}{\rho_0\omega}\frac{\partial p}{\partial x} \quad (23)$$

$$w = \frac{-i}{\rho_0\omega}\frac{\partial p}{\partial z} \quad (24)$$

When we substitute (23) and (24) back into the continuity equation (18) we obtain

$$-\nabla^2 p + \rho_0\omega\frac{\partial w}{\partial z} = 0 \quad (25)$$

where  $\nabla^2 = \frac{\partial^2}{\partial x^2} + \frac{\partial^2}{\partial z^2}$ . We can eliminate the pressure term  $\mathbf{p}' = (p_x, p_y, p_z) = \rho(i\omega u, i\omega v, i\omega w - \frac{\rho g}{\rho_0})$  by taking the second derivative  $\mathbf{p}'' = \rho(-\omega^2 u, -\omega^2 v, -\omega^2 w - \frac{g}{\rho_0}\frac{\partial\rho}{\partial z})$ . With these terms we can return to our basic equations and formulate the stream function.

### 2.3 Stream Function

In two dimensions, incompressible fluid motion can be modelled by a mathematical construct called the stream function, which behaves similarly to a potential field in electromagnetism. The stream function is usually denoted by  $\psi(x, y)$  and its primary property is that its derivatives give the velocity field of the fluid, that is  $\psi_z = -u$  and  $\psi_x = w$ . We take the second derivative of the pressure and the first derivative of the pressure dependent velocity terms (23) and (24) and insert them into the continuity equation (18). If we do this only in the  $u$  direction and eliminate the  $y$ -component, we obtain

$$\rho_0(N^2 - \omega^2)u_x - \omega^2\rho_0u_z = 0 \quad (26)$$

Replacing velocity fields  $(u, w)$  with the stream function, we get

$$(N^2 - \omega^2)\psi_{zz} - \omega^2\psi_{xx} = 0, \quad (27)$$

or

$$\left(\frac{N^2 - \omega^2}{\omega^2}\right)\psi_{xx} - \psi_{zz} = 0. \quad (28)$$

This automatically satisfies the incompressibility condition, the mass-conservation equation, and the momentum equation. This is the final result for the governing equation for the internal gravity waves. Equation (28) is a hyperbolic equation if  $(N^2 - \omega^2)$  is negative. We make the assumption that this is true as well as that  $N^2$  is more or less constant.

## 2.4 Delta Function and the Source Function

The Dirac delta function  $\delta(x)$  is a mathematical construct and a useful tool in the study of internal waves and other physical phenomena. The Delta function is usually used to describe a sudden pulse of a very short, near infinitesimal duration, which nevertheless transmits finite amounts of energy. For example, a simple pendulum in a viscous fluid subject to a sudden jolt at time  $t = 0$  is described by the equation :

$$\frac{d^2y}{dt^2} - ky + \omega^2y = \delta(t) \quad (29)$$

Function  $y(t)$  obtained as the solution of a differential equation (29) is typically called the impulse response or delta function response. In various branches of physics and engineering one frequently encounters a need to sample an arbitrary function at specific points along the time or space axis. This need is also met by the Dirac's  $\delta$ -function.

The primary property of the  $\delta$ -function is usually defined through the integral equation:

$$\int_{-\infty}^{\infty} \delta(x)f(x)dx = f(0) \quad (30)$$

Function  $\delta(x)$  "samples" the other function under the sign of integral  $f(x)$  at point  $x = 0$ . To sample function

$f(x)$  at point  $x = a$ , we would use the delta function  $\delta(x - a)$ , defined by the expression

$$\int_{-\infty}^{\infty} \delta(x - a)f(x)dx = f(a) \quad (31)$$

Equations (30) and (31) demonstrate some other important features of the delta function. From (30),( 31), we see that the domain of the  $\delta$ -function is infinitely narrow. If function  $f(x)$  has a value 0 at  $x = 0$ , integral (29) will simply give:

$$\int_{-\infty}^{\infty} \delta(x)f(x)dx = f(0) = 0 \quad (32)$$

irrespective of the value of  $f(x)$  at  $x = \epsilon$  arbitrarily close to  $x = 0$ . In spite of its infinitely narrow range, the integral over the  $\delta$  - function is finite and is actually equal to 1. We can see that if we set  $f(x) = 1$ , in equation (30), and we obtain

$$\int_{-\infty}^{\infty} \delta(x)dx = 1 \quad (33)$$

The above deliberations imply that  $\delta(x) = 0$ , for  $x \neq 0$ ,and  $\delta(0) = \infty$ . This means that  $\delta$ -function is not a continuous function.

Equation (31) demonstrates what is sometimes called shifting or translation property of the  $\delta$ -function. The translated  $\delta$ -function,  $\delta(x - a)$ , samples the applied function at the point  $x = a$ . We can define the same property through a shift in  $f(x)$ , namely:

$$\int_{-\infty}^{\infty} \frac{1}{|a|}\delta(x')f(x' + a)dx' = f(a) \quad (34)$$

Scaling the argument  $x$  of the  $\delta$ -function, i.e. using  $\delta(ax)$  results in the rescaling of the sampled value

$$\int_{-\infty}^{\infty} \delta(ax)f(x)dx = \int_{-\infty}^{\infty} \delta(x)f\left(\frac{x}{a}\right)dx = \frac{1}{|a|}f(0)$$

where we used a change of variables under the sign of the integral.

A similar property determines the value of the delta function that is a function of another function, namely  $\delta(g(x))$ . Again, through the change of variables under the sign of integral, one can show that:

$$\int_{-\infty}^{\infty} \delta(g(x))f(x)dx = \frac{1}{|dg/dx|}f(x_g)$$

Argument  $x_g$  is the value that makes function  $g(x)$  go to zero, i.e.  $g(x_g) = 0$ . The value of the derivative  $|dg/dx|$  is calculated at the point where  $g(x)$  goes through zero. If function  $g(x)$  has several zeros, the above expression transforms into a sum over all of them.

In order to develop a more rigorous foundation for the  $\delta$ -function one ought to consider it as the limit of a series of regular, continuous, functions. This will prove to be critical in applying perturbation theory to our system later on. It turns out that that can be accomplished in many ways. For example, we can introduce a series of continuous functions  $f_n$  defined on the  $x$ -axis as

$$f_n(x) = \frac{1}{\pi} \frac{n}{1 + n^2 x^2}$$

Each one of these functions, for any value of integer  $n$ , is a smooth, continuous function. For large values of  $n$  at any  $x$ , each of those functions has a vanishingly small value of the order of  $1/(\pi n x^2)$ . Near  $x = 0$ , those functions assume value  $n/\pi$ . In other words, for very large  $n$  and  $x \neq 0$ ,  $\lim_{n \rightarrow \infty} f_n(x) = 0$ , while at  $x = 0$ ,  $f_n(0) = n/\pi$ . Thus functions  $f_n(x)$  very much resemble  $\delta$ -function. We can express the last statement more formally as:

$$\lim_{n \rightarrow \infty} f_n(x) = 0, \quad x \neq 0$$

$$\lim_{n \rightarrow \infty} f_n(0) = \infty, \quad x = 0$$

Furthermore, the integral from  $-\infty$  to  $\infty$  over every one of functions  $f_n(x)$  is equal to 1, i.e.

$$\int_{-\infty}^{\infty} f_n(u) du = \lim_{x \rightarrow \infty} \int_{-x}^x f_n(u) du = \lim_{x \rightarrow \infty} \left( \frac{1}{2} + \frac{1}{\pi} \arctan(nx) \right) = 1, \quad \forall n \quad (35)$$

In other words, in the limit of large  $n$ , function  $f_n(x)$  behave very much like the  $\delta$ -function, they both vanish for any  $x$  which is different from  $x = 0$ , but become very large (infinite), at  $x = 0$  and have a finite value, i.e. 1, under an integral from  $-\infty$  to  $\infty$ .

One can also prove that the integral over the product of function  $f_n(x)$  and an arbitrary continuous integrable function  $g(x)$  will sample the value of function  $g(x)$  at  $x = 0$ , i.e.

$$\lim_{n \rightarrow \infty} \int_{-\infty}^{\infty} g(x) f_n(x) dx = g(0)$$

Which allows us to write:

$$\lim_{n \rightarrow \infty} f_n(x) = \lim_{n \rightarrow \infty} \frac{1}{\pi} \frac{n}{1 + n^2 x^2} = \delta(x)$$

Finally, one might wonder whether one can treat the  $\delta$ -function as an ordinary function and perhaps calculate its indefinite integral, derivatives or Taylor expansion. With some caution, the answer is affirmative on all counts.

The indefinite integral of the  $\delta$ -function has well defined properties. If  $x < 0$ , that integral is equal to 0. If  $x > 0$ , the integral is equal to 1 (33). The value of the integral can be defined in some fashion for  $x = 0$  as well. These observations come directly from the basic properties of the  $\delta$ -function. A function which is equal to 0 for negative values of  $x$  and equal to 1 for positive values of  $x$  is called the Heaviside function  $H(x)$ , therefore:

$$\int_{-\infty}^x \delta(x)dx = H(x) \quad (36)$$

Determination of the derivative of the  $\delta$ -function asks for somewhat more elaborate analysis. Suppose that the derivative of the  $\delta$ -function is defined and denoted by  $\delta'(x)$ . The integral from  $-\infty$  to  $\infty$  over a product of  $\delta'(x)$  and an arbitrary integrable and differentiable function  $f(x)$  given by  $\int_{-\infty}^{\infty} \delta'(x)f(x)dx$  can be calculated through integration by parts. We write:

$$\int_{-\infty}^{\infty} \delta'(x)f(x)dx = \delta(x)f(x)|_{x=-\infty}^{x=+\infty} - \int_{-\infty}^{\infty} \delta(x)f'(x)dx = - \int_{-\infty}^{\infty} \delta(x)\frac{d}{dx}f(x)dx \quad (37)$$

The first terms vanish since the delta function is zero at infinity. The first derivative of the delta function is equal to the negative value of the delta function multiplied from the right by the operator of the first derivative with respect to  $x$ . That operator will act on function  $f(x)$  under the sign of the integral. Therefore, we can write:

$$\delta'(x) = -\delta(x)\frac{d}{dx} \quad (38)$$

The second and every higher derivative could be calculated using the same approach. Hence,

$$\delta^{(n)}(x) = (-1)^n \delta(x)\frac{d^n}{dx^n} \quad (39)$$

The Taylor expansion of the  $\delta$ -function likewise reads,

$$\delta(x) = \sum_{n=0}^{\infty} \delta(0)(-1)^n \frac{1}{n!} \frac{d^n}{dx^n} = \delta(0)e^{ax} \quad (40)$$

Using these unique properties of the Delta function will be critical in solving for the source function  $\gamma(x, z)$  later on.

## 2.5 WKB Approximation and Green Function

We know that the density  $\rho_0$  and the buoyancy frequency  $N(z)$  vary slowly, i.e. their fractional change over a wavelength of wave motion in the vertical direction is much less than unity, we can use the WKB approximation to solve equation (27) for the stream function. We look for a solution to the equation

$$\frac{d^2 w}{dz^2} + m^2 w = 0, \quad (41)$$

where  $m^2 = \frac{N^2 - \omega^2}{\omega^2} k_x^2$ , in the form of

$$w = A(z) e^{i\phi(z)}, \quad (42)$$

where the phase  $\phi$  and the slowly varying amplitude  $A(z)$  are real. When we insert (42) into equation (41), we get

$$\frac{d^2 A}{dz^2} + A \left[ m^2 - \left( \frac{d\phi}{dz} \right)^2 \right] + i2 \frac{dA}{dz} \frac{d\phi}{dz} + iA \frac{d^2 \phi}{dz^2}. \quad (43)$$

Both the real and imaginary parts of equation (2.5) have to be equal to zero, which gives two equations.

$$\frac{d^2 A}{dz^2} + A \left[ m^2 - \left( \frac{d\phi}{dz} \right)^2 \right] = 0, \quad \text{and} \quad 2 \frac{dA}{dz} \frac{d\phi}{dz} + A \frac{d^2 \phi}{dz^2} = 0. \quad (44)$$

We assume that in the horizontal direction our solution will be a harmonic function of the form  $e^{ik_x x}$  and will have a frequency  $\omega$  of the lunar tide, i.e. be proportional to  $e^{-i\omega t}$ . Substituting in  $\Psi(x, z, \omega) = e^{i(k_x x)} a(z)$  into equation (28) gives us,

$$\frac{d^2}{dz^2} a(z) + \frac{N^2 - \omega^2}{\omega^2} k_x^2 a(z) = 0. \quad (45)$$

In first equation of (44) the term  $d^2 A/dz^2$  is negligible since the amplitude of waves is changing very little over the scale of one wavelength.

The real part of the WKB equation then approximately becomes equal to

$$\frac{d\phi}{dz} = \pm m, \quad (46)$$

with solution

$$\phi = \pm \int^z m dz, \quad (47)$$

with an arbitrary lower limit of the integral.

The amplitude is determined by writing the imaginary component of equation ( ) in the form

$$\frac{dA}{A} = -\frac{(d^2\phi/dz^2)dz}{2(d\phi/dz)} = -\frac{1}{2} \frac{dm}{m} \quad (48)$$

Integrating, we obtain  $\log A = \frac{1}{2} \log m + C$ , i.e.  $A = A_0/\sqrt{m}$ , where  $A_0$  is a constant. The WKB solution for the vertical velocity  $w$  is therefore

$$w = \frac{A_0}{\sqrt{m}} e^{\pm i \int^z m dz} \quad (49)$$

We can introduce the vertically averaged buoyancy frequency and the non-dimensional buoyancy frequency:

$$\bar{N} \equiv \frac{1}{H} \int_0^h N(z') dz', \quad \mathcal{N}(z) \equiv N(z)/\bar{N}. \quad (50)$$

The WKB stretched coordinate is defined as

$$Z \equiv \frac{\pi}{h} \int_0^h \mathcal{N}(z') dz', \quad (51)$$

where  $0 < Z < \pi$ . With this notation the WKB approximation to the eigenfunctions can be expressed as

$$a_n(z) \approx \frac{\sin(nZ)}{\sqrt{\mathcal{N}}}. \quad (52)$$

Following Smith and Young [8], we also find that  $c_n \approx h\bar{N}/n\pi$  and  $\bar{\omega}_n \approx \frac{1}{2}\bar{N}^2 h$ .

## 2.6 Green's Function in the WKB Approximation

In order to formulate a solution for the equation of motion (28) we need a Green function that satisfies the equation

$$\left( \frac{N^2 - \omega^2}{\omega^2} \right) G_{xx} - G_{zz} = \delta(x - x') \delta(z - z'). \quad (53)$$

subject to the radiation condition in  $x$  direction. The radiation condition implies that all disturbances must propagate away from  $x'$ , which requires that, for a horizontal wave number  $k$ , the Green function takes the form

$$G(x, x'; z, z')e^{-i\omega t} = f(k|x - x'| - \omega t); \quad (54)$$

It must also satisfy the homogeneity conditions in the vertical direction, i.e.

$$G(x, x'; 0, z') = G(x, x'; H, z') = 0 \quad (55)$$

Using the vertical normal modes obtained with WKB approximation, the Green function becomes

$$G(x, x'; z, z') = G_0 \sum_{n=1}^{\infty} \frac{e^{i\kappa_n|x-x'|}}{2i\kappa_n\bar{\omega}_n} a_n(z)a_n(z'), \quad (56)$$

with  $\kappa_n \equiv \frac{\sqrt{\omega^2}}{c_n}$ . The  $|x - x'|$  in the exponential on the right-hand side of (56) ensures that radiation is outgoing on both sides of the source at  $x - x' = 0$ .

From the WKB approximation we find that  $\kappa_n \approx n\pi/\mu h$ , where

$$\mu \equiv \frac{\bar{N}}{\sqrt{\omega^2}} \quad (57)$$

If we introduce the normalization parameters  $X \equiv \pi x/\mu h$  and  $Z \equiv \pi z/h$ , the WKB approximation of the Green function becomes

$$G_{WKB}(X, X'; Z, Z') = \sum_{n=1}^{\infty} \frac{\sin(nZ)\sin(nZ')}{n\pi\sqrt{\mathcal{N}(z)\mathcal{N}'(z')}} e^{in|X-X'|}. \quad (58)$$

The above summation was shown by Robinson [14] to be equal to,

$$G_{WKB}(x - x'; z, z') = \frac{1}{4\pi} \frac{1}{\sqrt{\mathcal{N}}\sqrt{\mathcal{N}'}} [\ln|\sigma| + i\pi H(-\sigma)] \quad (59)$$

where

$$\sigma(X - X'; Z, Z') \equiv \frac{\sin(\frac{1}{2}(|X - X'| + Z + Z')) \sin(\frac{1}{2}(|X - X'| - Z - Z'))}{\sin(\frac{1}{2}(|X - X'| + Z - Z')) \sin(\frac{1}{2}(|X - X'| - Z + Z'))} \quad (60)$$

and  $\mathcal{N}' \equiv \mathcal{N}(z')$  and  $H$  is the Heaviside step function. In our calculations we will be using both the logarithmic (60) and series solution (58) for the Green's function.

### 3 Source Function $\gamma(x, y)$ for the Triangular Ridge

We are here trying to establish a procedure for determining for the source function  $\gamma(x, y)$  along the triangular ridge, as defined by Smith, Young, and Pétélis works [13], [8]. We will start by defining the integral equation which expresses the stream function as a convolution of the source function and a Green's function. We will analyze the problem using perturbation theory. The zeroth order term and the unknown source function are the solutions for the knife edge solution as obtained by Young. The first order analysis accounts for the effect of a finite width of the ridge as well as ridge asymmetry.

#### 3.1 Solving the Integral Equation

The integral equation for the unknown source function  $\gamma(x, y)$ , in its most general form, reads as

$$\phi(x, z) = \int_{y_0}^{y_1} \int_{x_0}^{x_1} \gamma(x', z') G_{WKB}(x, x'; z, z') dx' dz'$$

where  $\phi(x, z)$  is the stream function at points away from the ridge. The integral follows the contour of the ridge. For an infinitely thin edge, we redefine the source density as  $\gamma(x, z) = \delta(x)\hat{\gamma}(z)$ , where  $\hat{\gamma}(z) = \gamma(z)$  for  $z = [0, b]$  and zero otherwise, where  $b$  is the height of the ridge. This reduces the integral equation to that found in Robinson and Young, that is:

$$\phi(x, z) = \int_0^b \int_{x_0}^{x_1} \delta(x')\hat{\gamma}(z') G_{WKB}(x, x'; z, z') dx' dz' = \int_0^b \hat{\gamma}(z') G_{WKB}(x, 0; z, z') dz'$$

For a triangular ridge we write the integral equation as did Pétrelis, that is,

$$\phi(x, z) = \frac{1}{2} \int_0^b \gamma(z') [G(x + q(z'); z, z') + G(x - q(z'); z, z')] dz'$$

where  $q(z')$  takes the place of  $x'$  to define the sloping edge of the symmetric triangular ridge,  $q(z') = a(1 - z'/b)$ .

Likewise, just to note, we can redefine the Green's function as  $G(x - x'; z, z')$  instead of  $G(x, x'; z, z')$  because in the WKB formulation  $x$  and  $x'$  everywhere appear in combination  $x - x'$ . When we insert the

WKB approximation for the Green's function  $G_{WKB}$  into the integral equation, we obtain

$$\phi(x, z) = \int_0^b \gamma(z') R(z, z') dz' \quad (61)$$

Here, following Pétrélis, we define the kernel  $R(z, z')$ , using the  $q = q(z)$ , as

$$R(z, z') = \frac{1}{2} G_{WKB}(q + q'; z, z') + \frac{1}{2} G_{WKB}(q - q'; z, z') = \frac{1}{2\pi} \sum_{n=1}^{\infty} \frac{1}{n} \sin(nZ) \sin(nZ') [e^{in(Q+Q')} + e^{in|Q-Q'|}]$$

The above integral follows the topography, i.e. the triangular edge. In the above equation,  $Q(Z) = \pi q(z)/\mu h$ ,  $X = \pi x/\mu h$ , and  $Z = \pi z/h$  are the nondimensional coordinates. If  $q = q' = 0$ , the integral equation collapse to that solved by Smith and Young for the knife edge. For the symmetric triangular ridge,  $Q(Z) = A(1 - \frac{Z}{B})$ , where  $A = \pi a/\mu h$  and  $B = \pi z/h$ .

In order to obtain an asymmetric triangle of finite width, i.e.  $x = [-a_1, a_2]$ , we redefine the source function into two branches,  $\gamma_- = \delta(x - q_-(z))\hat{\gamma}_-(z)$  and  $\gamma_+ = \delta(x - q_+(z))\hat{\gamma}_+(z)$ , where  $+$  and  $-$  define the right and left half-planes,  $x = [-a_1, 0]$  and  $x = [0, a_2]$ , respectively. The physical system is depicted in the following figure (1):

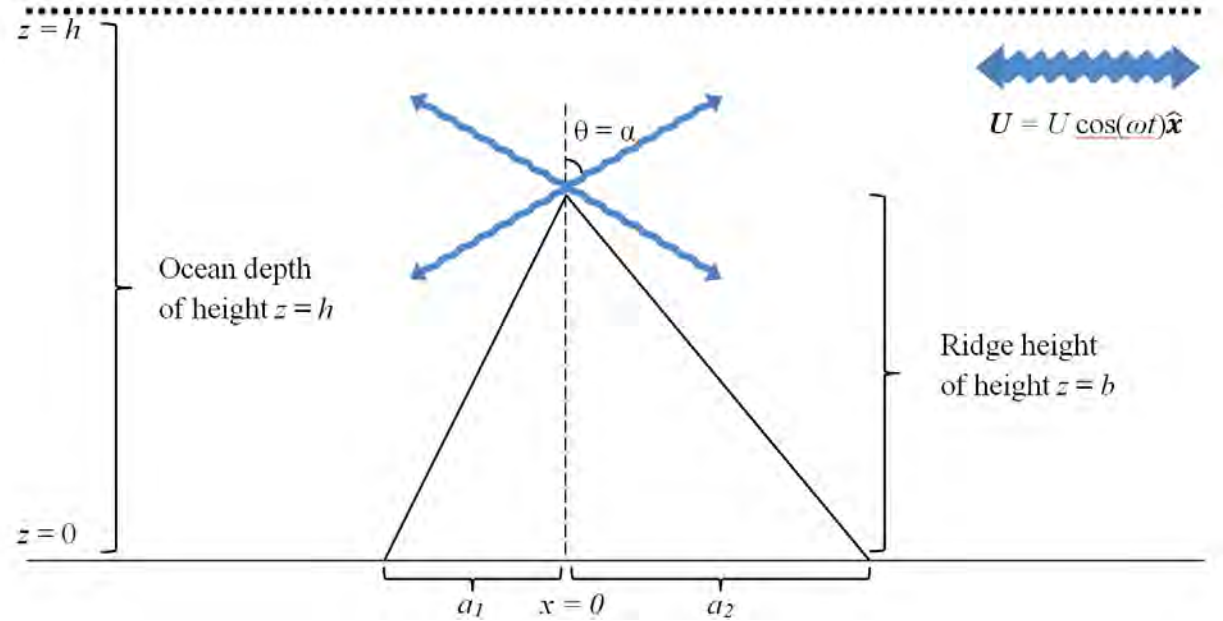


Figure 1: The physical system for which we will be solving the integral equation for the source  $\gamma(z)$ . The ocean is of a depth (or height in our coordinates) of  $z = h$  and the ocean bottom is at  $z = 0$ . The ridge is of a height  $b$  and has half-base lengths of  $a_1$  and  $a_2$ . The angle of internal wave emanation  $\theta = \alpha$ , as noted in equation (17). In addition, the tidal frequency is  $\mathbf{U}$ .

Our topography, an asymmetric triangular ridge, is defined by functions  $q_{\pm}(z) = x = a_{1,2}(1 \mp z/b)$ , where  $a_{1,2}$  are the half base lengths of the triangle measured from  $x = 0$ , left and right respectively, and  $b$  is the height. Written out explicitly, the integral equation for the asymmetric case becomes:

$$\phi(x, z) = \frac{1}{2} \int_0^b \int_{-a}^a [\delta(x - q_-(z))\gamma_-(z')G_{WKB}(x + x'; z, z') + \delta(x - q_+(z))\gamma_+(z')G_{WKB}(x - x'; z, z')] dx' dz'$$

After applying the  $\delta$ -function, effectively eliminating the  $x$ -integral, the previous equation reduces to

$$\phi(x, z) = \frac{1}{2} \int_0^b [\gamma_-(z')G_{WKB}(x + q'; z, z') + \gamma_+(z')G_{WKB}(x - q'; z, z')] dz'.$$

In our perturbation approach we are starting with kernel  $R(z, z') = \frac{1}{2}(\gamma_-G + \gamma_+G)$ , using equation (61) for the symmetric triangular ridge as defined by Pétrélis and then extending it to the asymmetric case. The first step of the perturbation analysis is to expand the kernel with respect to small term  $\epsilon = A/B = a/\mu b$ , giving us  $R(Z, Z') = R_0(Z, Z') + i\epsilon R_1(Z, Z') + \epsilon^2 R_2(Z, Z') - \mathcal{O}(\epsilon^3)$ .

We identify the small parameter  $\epsilon$  from the topography function,  $Q(Z) = A(1 - Z/B) = \frac{A}{B}(B - Z) = \epsilon Q(Z)$ . The terms in the perturbation expansion of  $R$  are,

$$R_0(Z, Z') = \frac{1}{2\pi} \ln \left| \frac{\sin\left(\frac{Z + Z'}{2}\right)}{\sin\left(\frac{Z - Z'}{2}\right)} \right| \quad (62)$$

$$R_1(Z, Z') = \frac{1}{4} Q(Z) \delta(Z - Z'), \quad (63)$$

$$R_2(Z, Z') = -\frac{1}{2\pi} [Q^2(Z) + Q^2(Z')] \sum_{n=1}^{\infty} \sin(nZ) \sin(nZ') \quad (64)$$

Next, we will show how we derived these terms before moving onto the calculation of the source function.

### 3.2 Perturbation Expansion of $R(Z, Z')$

The zeroth order term of the kernel in the expansion with respect to  $\epsilon$  is the Green's function for the knife edge around  $x = x' = 0$ , that is

$$R_0(Z, Z') = G_{WKB}(X, X'; Z, Z)|_{X=X'=0} = \frac{1}{4\pi} \ln \left| \frac{\sin(\frac{1}{2}(|0 - 0| + Z + Z')) \sin(\frac{1}{2}(|0 - 0| - Z - Z'))}{\sin(\frac{1}{2}(|0 - 0| + Z - Z')) \sin(\frac{1}{2}(|0 - 0| - Z + Z'))} \right|$$

$$= \frac{1}{4\pi} \ln \left| \frac{\sin(\frac{1}{2}(Z + Z')) \sin(\frac{1}{2}(-Z - Z'))}{\sin(\frac{1}{2}(Z - Z')) \sin(\frac{1}{2}(-Z + Z'))} \right| = \frac{1}{4\pi} \ln \left| \frac{\sin^2(\frac{1}{2}(Z + Z'))}{\sin^2(\frac{1}{2}(Z - Z'))} \right| = \frac{1}{2\pi} \ln \left| \frac{\sin(\frac{1}{2}(Z + Z'))}{\sin(\frac{1}{2}(Z - Z'))} \right|$$

The first order term is slightly more complicated. Instead of the logarithmic expression we start with the series summation for the Green's function.

$$\begin{aligned} R_1(Z, Z') &= \frac{d}{d\epsilon} G_{WKB}(X, X'; Z, Z')|_{X=X'=0} = \frac{1}{2} \frac{i}{2\pi} \sum_{n=1}^{\infty} \sin(nZ) \sin(nZ') [\mathcal{Q}(Z) + \mathcal{Q}(Z') + \mathcal{Q}(Z) - \mathcal{Q}(Z')] \\ &= \frac{i}{2\pi} \sum_{n=1}^{\infty} \sin(nZ) \sin(nZ') \mathcal{Q}(Z) \end{aligned}$$

From some simple testing we can observe that  $\sum_{n=1}^{\infty} \sin(nZ) \sin(nZ') = 0$  when  $z \neq z'$ , but for  $z = z'$ ,  $\sum_{n=1}^{\infty} \sin(nZ)^2$  diverges. From our discussion of the  $\delta$ -function we see how this matches the basic property of that function. However, we can be more rigorous and prove that, i.e.

$$\sum_{n=1}^{\infty} \sin(nZ) \sin(nZ') = -\frac{\pi}{2} \delta(Z - Z') \quad \text{when } Z, Z' > 0.$$

Expanding the trigonometric terms into exponentials we write:

$$\begin{aligned} \sum_{n=1}^{\infty} \sin(nZ) \sin(nZ') &= -\frac{1}{4} \sum_{n=1}^{\infty} (e^{inZ} - e^{-inZ})(e^{inZ'} - e^{-inZ'}) \\ &= -\frac{1}{4} \sum_{n=1}^{\infty} (e^{in(Z+Z')} + e^{-in(Z+Z')} - e^{-in(Z-Z')} - e^{in(Z-Z')}) \end{aligned}$$

Noticing the fact that negative values of  $n$  effectively switches the direction of the summation of the series, we can concisely rewrite the above formulation as

$$= -\frac{1}{4} \sum_{n=-\infty}^{\infty} e^{in(Z+Z')} + \frac{1}{4} - \frac{1}{4} \sum_{n=-\infty}^{\infty} e^{in(Z-Z')} - \frac{1}{4}$$

Considering one of the expansions of the  $\delta$ -function,  $\frac{1}{2\pi} \sum_{n=-\infty}^{\infty} e^{inx} = \delta(x)$ , we can rewrite the previous

result as:

$$-\frac{\pi}{2} \frac{1}{2\pi} \sum_{n=-\infty}^{\infty} e^{in(Z+Z')} - \frac{\pi}{2} \frac{1}{2\pi} \sum_{n=-\infty}^{\infty} e^{in(Z-Z')} \Rightarrow -\frac{\pi}{2} \delta(Z+Z') - \frac{\pi}{2} \delta(Z-Z') = -\frac{\pi}{2} (\delta(Z+Z') + \delta(Z-Z'))$$

Since both  $Z$  and  $Z' > 0$ , we know that  $\delta(Z+Z') \equiv 0$ .  $\delta(z+z')$  can never sample a coordinate  $Z' < 0$  in our system necessary for it to give non-zero value. Therefore, the first order correction term reduces to

$$R_1(Z, Z') = -\frac{i}{4} Q(Z) \delta(Z-Z')$$

The second order term,  $R_2$ , was not used in this study. Nevertheless we will present its value for the benefit of some future work. The second order term is similarly derived from the summation form of the Green's function.

$$R_2(Z, Z') = -\frac{1}{4} \frac{1}{2\pi} \sum_{n=-1}^{\infty} n \sin(nZ) \sin(nZ') [(\mathcal{Q}(Z) + \mathcal{Q}(Z'))^2 + (\mathcal{Q}(Z) - \mathcal{Q}(Z'))^2]$$

This term diverges near  $Z = Z'$  but is necessary for calculating the conversion rate  $M$  for topographies such as the polynomial ridge in P  tr  lis' paper.

### 3.3 Zeroeth Order Term of the Source Function $\gamma_0(z)$

Now that we have the expansion for the kernel  $R(Z, Z')$  we may solve for the source function. The source function is expanded in the same small parameter  $\epsilon$ . That is,

$$\gamma(z) = \gamma_0(z) - \epsilon \gamma_1(z) + \epsilon^2 \gamma_2(z) - \mathcal{O}(\epsilon^3).$$

We now introduce expansions of  $R(Z, Z')$  and  $\gamma(z)$  into the integral equation (61) and collect terms in powers of  $\epsilon$ . This giving us a hierarchy of integral equations:

$$\int_0^B R_0(Z, Z') \gamma_0(Z') dZ' = Z, \tag{65}$$

$$\int_0^B R_0(Z, Z')\gamma_1(Z')dZ' = - \int_0^B R_1(Z, Z')\gamma_0(Z')dZ', \quad (66)$$

$$\int_0^B R_0(Z, Z')\gamma_2(Z')dZ' = \int_0^B R_1(Z, Z')\gamma_1(Z')dZ' - \int_0^B R_2(Z, Z')\gamma_0(Z')dZ'. \quad (67)$$

The above a hierarchy of equations can be solved for the source function for each order individually, starting with the zeroeth order.

To calculate the zeroeth order approximation of the source function  $\gamma'$  we insert  $R_0$  into the integral equation (65). Considering the property of the logarithm,  $\ln(\frac{a}{b}) = \ln(a) - \ln(b)$ , we write

$$\int_0^B \frac{1}{2\pi} \ln \left| \frac{\sin(\frac{1}{2}(Z + Z'))}{\sin(\frac{1}{2}(Z - Z'))} \right| \gamma_0(Z')dZ' =$$

$$\int_0^B \frac{1}{2\pi} \left[ \ln \left| \sin \left( \frac{1}{2}(Z + Z') \right) \right| - \ln \left| \sin \left( \frac{1}{2}(Z - Z') \right) \right| \right] \gamma_0(Z')dZ' = Z. \quad (68)$$

Following the procedure proposed by Young, we take the first derivative of the equation (68)with respect to  $Z$ , which gives:

$$2 = \int_0^B \gamma_0(Z') \left[ \frac{\sin(Z')}{\cos(Z) - \cos(Z')} \right] \frac{dZ'}{\pi}.$$

This is the airfoil equation, which is well known from classical fluid mechanics. Following Young, we change variables  $Z$  and  $Z'$  to variable  $\nu$  and  $\nu'$ .  $\nu$  defined in terms of  $Z$  reads:

$$\nu = 2 \frac{1 - \cos(Z)}{1 - \cos(B)} - 1, \quad d\nu = 2 \frac{\sin(Z)}{1 - \cos(B)} dZ \quad (69)$$

$\nu'$  has an identical dependence on  $Z'$ . Equation (69) can be transformed into:

$$\cos(Z) = 1 - \frac{1}{2}(\nu + 1)(1 - \cos(B)) = 1 - \frac{1}{2}(\nu - \nu \cos(B) + 1 - \cos(B)) \quad (70)$$

Inserting equations (69) into the airfoil equation and letting  $\Upsilon_0(\nu) = \gamma_0(Z)$  we obtain

$$2 = \int_{-1}^1 \frac{\Upsilon_0(\nu') \sin(Z')}{\cos(Z) - \cos(Z')} \frac{(1 - \cos(B)) d\nu'}{2 \sin(Z')} \frac{1}{\pi} = \frac{1}{2} \int_{-1}^1 \frac{\Upsilon_0(\nu')(1 - \cos(B))}{\cos(Z) - \cos(Z')} \frac{d\nu'}{\pi}$$

With the help of equation (70), this transforms further into:

$$\begin{aligned}
2 &= \frac{1}{2} \int_{-1}^1 \frac{\Upsilon_0(\nu')(1 - \cos(B))}{1 - \frac{1}{2}(\nu + 1)(1 - \cos(B)) - 1 + \frac{1}{2}(\nu' + 1)(1 - \cos(B))} \frac{d\nu'}{\pi} \\
&= \frac{1}{2} \int_{-1}^1 \frac{\Upsilon_0(\nu')(1 - \cos(B))}{-\frac{1}{2}(\nu + 1)(1 - \cos(B)) + \frac{1}{2}(\nu' + 1)(1 - \cos(B))} \frac{d\nu'}{\pi} \\
&= \frac{1}{2} \int_{-1}^1 \frac{\Upsilon_0(\nu')(1 - \cos(B))}{-\frac{1}{2}(\nu + 1 - \nu' - 1)(1 - \cos(B))} \frac{d\nu'}{\pi} \\
2 &= \frac{1}{\pi} \int_{-1}^1 \frac{\Upsilon_0(\nu')}{(\nu - \nu')} d\nu' \tag{71}
\end{aligned}$$

This is a special case of the airfoil equation - a Cauchy singular integral equation of the first kind. To solve this equation we use the finite Hilbert transform.

### 3.4 Finite Hilbert transform for the airfoil equation

To solve equation (71) we can use the general approach for the inversion of a finite Hilbert transform on an integration range  $[a, b]$ , which is the solution for the following equation.

$$g(x) = \frac{1}{\pi} P.V. \int_a^b \frac{f(t)}{x-t} dt, \quad \text{with } a < x < b$$

Where  $P.V.$  is the Cauchy Principal value. Let the transform operation in equation (71)  $\frac{1}{\pi} P.V. \int_a^b \frac{f(t)}{x-t} dt$  be denoted by  $T_{ab}$ , so that

$$T_{ab}f(\nu) = g(\nu)$$

Three relationships are useful for solving equation (71):

$$T_{ab}\left[\frac{1}{\sqrt{(b-\nu)(\nu-a)}}\right] = 0 \tag{72}$$

$$T_{ab}\left[\frac{\nu}{\sqrt{(b-\nu)(\nu-a)}}\right] = -1 \tag{73}$$

$$T_{ab}\left[\sqrt{(b-\nu)(\nu-a)}\right] = \nu - \frac{b+a}{2} \tag{74}$$

Subsequently, the Tricomi identity for the operator  $T_{ab}$  is employed. For two functions  $\phi_1$  and  $\phi_2$  with supports in the interval  $(a, b)$ , where  $\phi_1 \in L^{p_1}(a, b)$  and  $\phi_2 \in L^{p_2}(a, b)$ , with  $p_1 > 1, p_2 > 1$ , and  $p_1^{-1} + p_2^{-1} \leq 1$ , it follows that

$$T_{ab}[\phi_1(\nu')T_{ab}\phi_2(\nu') + \phi_2(\nu')T_{ab}\phi_1(\nu')] = T_{ab}\phi_1(\nu)T_{ab}\phi_2(\nu) - \phi_1(\nu)\phi_2(\nu) \quad (75)$$

We can make certain choices made regarding function  $\phi_1(\nu)$  and  $\phi_2(\nu)$ . For example, we can select:

$$\phi_1(\nu) = f(\nu), a < \nu < b, \text{ otherwise } 0 \text{ and } \phi_2(\nu) = \sqrt{(b-\nu)(\nu-a)}, a < \nu < b, \text{ otherwise } 0$$

Let  $g(x) = T_{ab}f(x)$ . With these choices, from equation (75) we read that

$$f(\nu) = \frac{g(\nu)T_{ab}[\sqrt{(b-\nu)(\nu-a)}]}{\sqrt{(b-\nu)(\nu-a)}} - \frac{T_{ab}[f(\nu)T_{ab}[\sqrt{(b-\nu)(\nu-a)}] + g(\nu)\sqrt{(b-\nu)(\nu-a)}]}{\sqrt{(b-\nu)(\nu-a)}}$$

This simplifies upon using equation (74) to give

$$\begin{aligned} f(x) &= \frac{g(x)[x - (b+a)/2]}{\sqrt{(b-x)(x-a)}} - \frac{T_{ab}[f(x)[x - (b+a)/2] + g(x)\sqrt{(b-x)(x-a)}]}{\sqrt{(b-x)(x-a)}} \\ &= \frac{xg(x)}{\sqrt{(b-x)(x-a)}} - \frac{T_{ab}[xf(x)]}{\sqrt{(b-x)(x-a)}} - \frac{T_{ab}[g(x)\sqrt{(b-x)(x-a)}]}{\sqrt{(b-x)(x-a)}} \end{aligned}$$

Using the moment formula for the finite Hilbert transform,

$$T_{ab}[xf(x)] = xT_{ab}f(x) - \frac{1}{\pi} \int_a^b f(x)dx \quad (76)$$

and setting

$$\Lambda = \frac{1}{\pi} \int_a^b f(x)dx$$

allows equation (76) to be simplified further into:

$$f(x) = \frac{\Lambda}{\sqrt{(b-x)(x-a)}} - \frac{T_{ab}[g(x)\sqrt{(b-x)(x-a)}]}{\sqrt{(b-x)(x-a)}} \quad (77)$$

After inserting the values  $a = -1, b = 1$ , and  $g(x) = -2$ , we get

$$\Upsilon_0(\nu) = \frac{\Lambda}{\sqrt{1-\nu^2}} - \frac{2\nu}{\sqrt{1-\nu^2}} = \frac{(\Lambda + 2\nu)}{\sqrt{1-\nu^2}}$$

Following Young, to determine  $\Lambda$  we argue that  $\gamma_0(Z)$  must be non-singular at  $Z = 0$ . This regularity condition implies that  $\Upsilon_0(\nu)$  must be non-singular at  $\nu = -1$  so that  $\Lambda = 2$ , giving us the solution for the zeroth order term for the source function:

$$\Upsilon_0(\nu) = 2 \frac{1+\nu}{\sqrt{1-\nu^2}} = 2 \frac{(\sqrt{1+\nu})^2}{\sqrt{1-\nu}\sqrt{1+\nu}} = 2 \frac{\sqrt{1+\nu}}{\sqrt{1-\nu}}, \quad \gamma_0(Z) = 2 \sqrt{\frac{1-\cos(Z)}{\cos(Z)-\cos(B)}}.$$

This is the solution for the knife edge. We can use that solution as the starting point in calculating the higher order terms, primarily the first order correction, in our case.

### 3.5 Calculation of the First Order Term $\gamma_1(z)$

Now that we have the zeroth order approximation to the source function we can return to the first order integral equation, (66)

$$\int_0^B R_0(Z, Z') \gamma_1(Z') dZ' = - \int_0^B R_1(Z, Z') \gamma_0(Z') dZ'$$

We now know  $\gamma_0$  in addition to  $R_0$  and  $R_1$ , allowing us to solve for the unknown function,  $\gamma_1$ , i.e. the first order correction to the source function. The full expression of above integral equation reads:

$$\int_0^B \frac{1}{2\pi} \frac{\ln \left| \frac{\sin(\frac{1}{2}(Z+Z'))}{\sin(\frac{1}{2}(Z-Z'))} \right|}{\ln \left| \frac{\sin(\frac{1}{2}(Z+Z'))}{\sin(\frac{1}{2}(Z-Z'))} \right|} \gamma_1(Z') dZ' = - \int_0^B \frac{1}{4} Q(Z) \delta(Z-Z') 2 \sqrt{\frac{1-\cos(Z')}{\cos(Z')-\cos(B)}} dZ' \quad (78)$$

Using the  $\delta$ -functions we are able to immediately simplify the equation by eliminating the integral on the right. The simplified expression (remembering that  $Q(Z) = B - Z$ ), reads:

$$\int_0^B \frac{1}{2\pi} \frac{\ln \left| \frac{\sin(\frac{1}{2}(Z+Z'))}{\sin(\frac{1}{2}(Z-Z'))} \right|}{\ln \left| \frac{\sin(\frac{1}{2}(Z+Z'))}{\sin(\frac{1}{2}(Z-Z'))} \right|} \gamma_1(Z') dZ' = -\frac{1}{2} (B-Z) \sqrt{\frac{1-\cos(Z)}{\cos(Z)-\cos(B)}} \quad (79)$$

This integral is still not simple enough to solve analytically, as we must still deal with the difficult Hilbert transform. In the case of the zeroth order term, our term for  $g(x)$  was merely a constant and we already had a simple formula at hand in identity (74) that greatly simplified the general solution to the finite Hilbert

transform of equation (77). For the first order term, equation (79),  $g(x)$  is not a constant. However, we may apply a realistic approximation that tolerably simplifies the problem.

The only systems in which internal waves are effectively observed are the deep oceans where there is large enough of a gradient in the water density, along the vertical axis. This allowed for the use of the weak topography approximation (WTA) that treats the height of obstacles as relatively insignificant as compared to the overall depth of the ocean. We will also use this approximation to help solve the first order equation (79). We assume that  $b \ll h$ , where  $h$  is the ocean depth and  $b$  is the height of the ridge. This in turn means that  $B \ll 1$ , reducing the  $\cos(B)$  in the above equation to effectively 1. Equation (79) now reduces to

$$\begin{aligned} \int_0^B \frac{1}{2\pi} \frac{\ln \left| \sin \left( \frac{1}{2}(Z + Z') \right) \right|}{\ln \left| \sin \left( \frac{1}{2}(Z - Z') \right) \right|} \gamma_1(Z') dZ' &= -\frac{1}{2}(B - Z) \sqrt{\frac{1 - \cos(Z)}{\cos(Z) - 1}} \\ &= -\frac{1}{2}(B - Z) \sqrt{\frac{1 - \cos(Z)}{-(1 - \cos(Z))}} = -\frac{1}{2}(B - Z) \sqrt{-1} = -\frac{i}{2}(B - Z) \end{aligned} \quad (80)$$

Now we can take the derivative with respect to  $Z$  (reapplying the technique Young used for the knife edge).

The result is:

$$\int_0^B \frac{1}{2\pi} \left[ \frac{\sin(Z')}{\cos(Z) - \cos(Z')} \right] \gamma_1(Z') dZ' = \frac{i}{2}$$

Since the right-handside is merely a constant we can easily apply formula (77) to give us a solution that is almost exactly the same as the knife edge except for a constant, that is

$$\gamma_1(Z) = \frac{i}{2} \sqrt{\frac{1 - \cos(Z)}{\cos(Z) - 1}} \quad (81)$$

When we add this correction term to the source function we get

$$\gamma(Z) = \gamma_0(Z) + i\epsilon\gamma_1(Z) = 2\sqrt{\frac{1 - \cos(Z)}{\cos(Z) - 1}} + i\epsilon\frac{i}{2}\sqrt{\frac{1 - \cos(Z)}{\cos(Z) - 1}} = 2\left(1 - \frac{1}{4}\epsilon\right)\sqrt{\frac{1 - \cos(Z)}{\cos(Z) - 1}} \quad (82)$$

This essentially says that the wider the ridge, i.e. the larger the perturbation term  $\epsilon$ , the weaker the source function.

## 4 Symmetric and Asymmetric Triangular Ridge

We pursued our earlier investigation in order to solve for the unknown source function  $\gamma(z)$  in the integral equation,

$$\phi(x, z) = \int_0^b \gamma(z')R(z, z')dz' \quad (83)$$

We found that the first order correction to the knife edge to be essentially the same solution multiplied by a constant. With this result we can investigate several phenomena related to internal waves.

### 4.1 Tidal Conversion Rate $M$

It is believed that internal waves play an important role in the energy balance of the ocean and mixing in the deep ocean. An important indicator of this is the tidal conversion rate  $M$ , which effectively tells us how much of tidal energy is converted into internal waves. The conversion rate is dependent on the source function, or more explicitly the topography. Converted tidal power can be expressed as

$$\mathcal{C} = \frac{\pi}{4}b^2\rho U^2 N \sqrt{1 - \frac{f^2}{\omega}} \times M\left(\frac{b}{h}, \frac{a}{\mu h}, \frac{\omega}{N}, \frac{U}{\omega a}, \dots\right), \quad (84)$$

where  $\rho$  is the average density of seawater,  $U$  is the maximum velocity of the tidal flow, and  $M$  is a dimensionless function. The units of  $\mathcal{C}$  are watts per meter of the ridge. In previous studies by Khatiwala (2003) or Smith and Young (2002), in the WTA approximation, the triangular ridge gave a solution for the function  $M$  of the form

$$M_{WTA}\left(\frac{a}{\mu h}\right) = \frac{32}{\pi^2 A^2} \sum_{n=1}^{\infty} n^{-3} \sin^4\left(\frac{nA}{2}\right). \quad (85)$$

Given that we are approaching the problem via the source function, we can calculate the conversion rate from the following equation:

$$M = \frac{2}{\pi B^2} \int_0^B dZ \int_0^B dZ' \gamma(Z)\gamma^*(Z')\mathcal{R}_r(Z, Z'). \quad (86)$$

Following Pétrélis' work and using the symmetry of  $\mathcal{R}(\mathcal{Z}, \mathcal{Z}') = \mathcal{R}(\mathcal{Z}', \mathcal{Z})$  we can eliminate the double

integral and write,

$$M = \frac{2}{\pi B^2} \int_0^B \gamma_r(Z) Z dZ \quad (87)$$

where  $\gamma_r(Z)$  is the real part of  $\gamma(Z)$ . According to Pétrélis and his numerical studies, we can expand the conversion function as a power series in  $\epsilon^2$ , i.e.  $M = M_{knife}(B) + \epsilon^2 M_2(B) + \mathcal{O}(\epsilon^4)$ . The first order conversion function is the same as as the above function, except with  $\gamma_0$  used for  $\gamma_r$ . This result was obtained by Smith and Young as well as Robinson. The second order term is a littler more complicated. According to Pétrélis, it is equal to

$$M_2 = \frac{1}{\pi B^2} \int_0^B \mathcal{Q}(Z) \gamma_0(Z) \gamma_1(Z) dZ - \frac{2}{\pi B^2} \int_0^B dZ \int_0^B dZ' \gamma_0(Z) \gamma(Z') \mathcal{R}_2(Z, Z') \quad (88)$$

Several simplifications can be made using the following formulas

$$\int \int \gamma_0(Z') \mathcal{R}_0(Z, Z') \gamma_2(Z) - \gamma_0(Z') \mathcal{R}_1(Z, Z') \gamma_1(Z) + \gamma_0(Z') \mathcal{R}_2(Z, Z') \gamma_0(Z) = 0, \quad (89)$$

$$\int \int \gamma_1(Z') \mathcal{R}_0(Z, Z') \gamma_1(Z) + \gamma_1(Z') \mathcal{R}_1(Z, Z') \gamma_0(Z) = 0, \quad (90)$$

and

$$\int_0^B \int_0^B \gamma_0(Z') \mathcal{R}_2(Z, Z') \gamma_0(Z) dZ dZ' = 0 \quad (91)$$

Applying these identities to equation (88) we get the final integral for  $M_2$ ,

$$M_2 = \frac{1}{\pi B^2} \int_0^B \mathcal{Q}(Z) \gamma_0(Z) \gamma_1(Z) = \frac{1}{\pi B^2} \int_0^B \pi(B - Z) \left( \frac{1 - \cos Z}{\cos Z - \cos B} \right) dZ \quad (92)$$

which we can calculate numerically. In addition to the correction term, we have

$$M_{knife} = \frac{2}{\pi B^2} \int_0^B Z \sqrt{\frac{1 - \cos(Z)}{\cos(Z) - \cos(B)}} dZ. \quad (93)$$

For the symmetric triangle we were able to generate two plots that help us understand the nature of the of the triangular ridge and its effects upon the conversion rate.

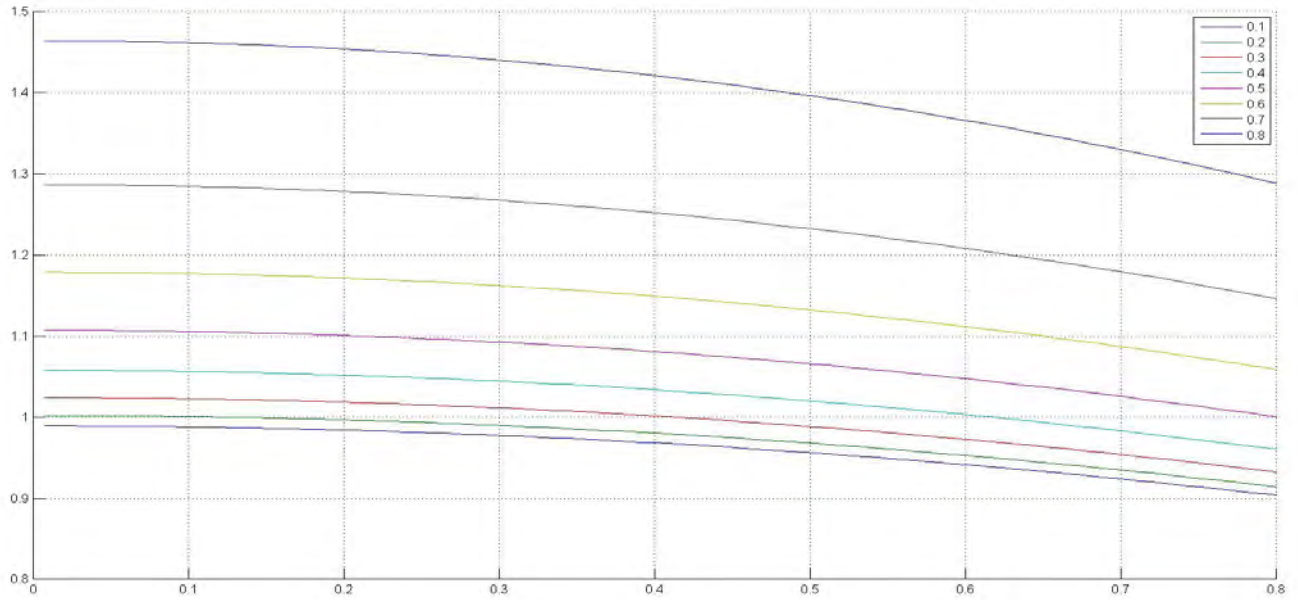


Figure 2: Conversion function  $M(B)$  as a function of  $\epsilon$ , with the various lines being representative of a varying ridge height  $B$ .

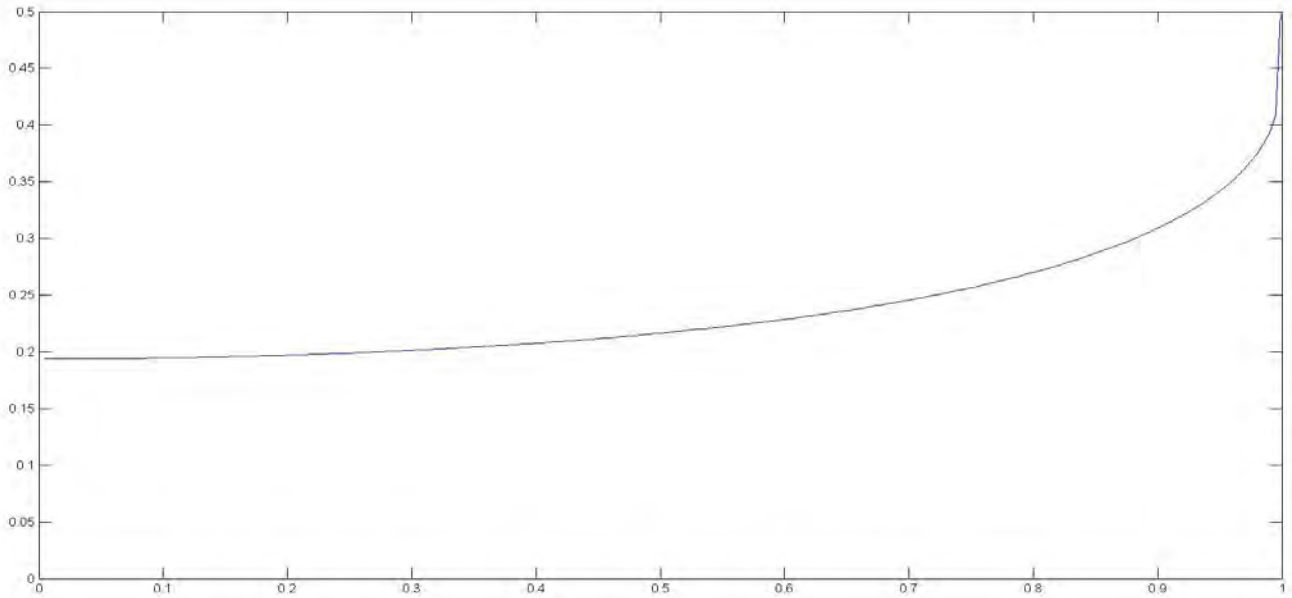


Figure 3: The ratio of the two components of the conversion function  $M_2(B)/M_{\text{knife}}$  as a function of  $B$ .

These two results compare well with results generated by Pétrélis in his 2003 work.

We can introduce asymmetry into our problem by slightly altering our equation for the conversion function,  $M = M_{knife}(B) + \frac{1}{2}(\epsilon_1^2 + \epsilon_2^2)M_2(B)$ , where  $\epsilon_1$  and  $\epsilon_2$  correspond to triangle base lengths  $a_1$  and  $a_2$ , respectively. This alteration behaves essentially the same as a variation in the ridge height  $B$ , as shown in the following figure for ridge height  $B = 0.8$ .

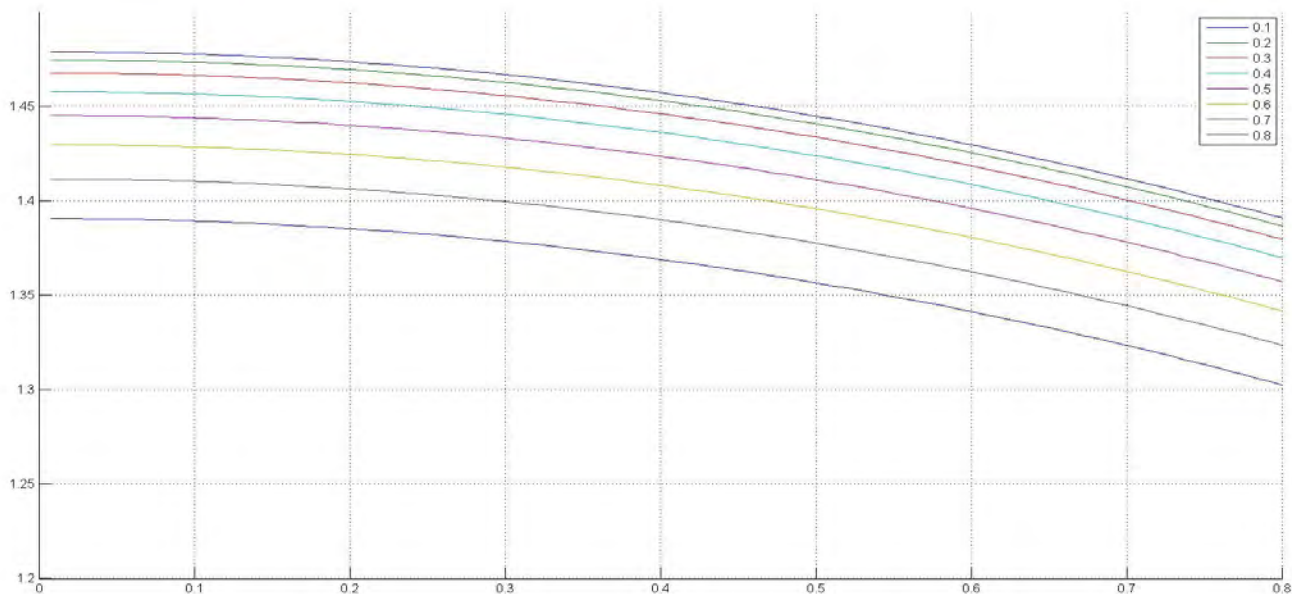


Figure 4: The ratio of the two components of the conversion function  $M_2(B)/M_{knife}$  as a function of  $B$ . Colored lines are for varying values of  $\epsilon_2$ , where  $\epsilon_1$  is fixed at 0.8.

Figure (4) effectively tells us that the more asymmetric the ridge the weaker the conversion rate, intuitively stemming from the earlier conclusion that the wider the ridge the weaker the conversion rate.

## 4.2 Stream Function $\phi(x, z)$

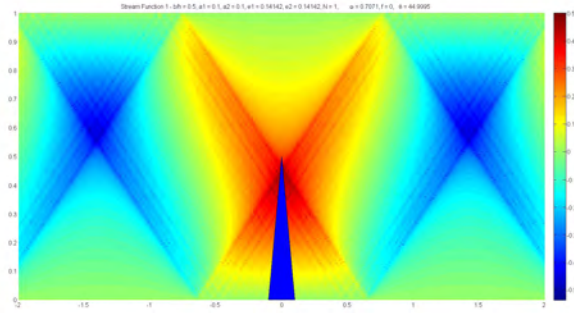
In general, the most expressive qualifier of an incompressible fluid flow is the stream function  $\phi(x, z)$ . With the source function  $\gamma(x, z)$  at hand, we can calculate the stream function for the entire field using the

full integral equation., that is:

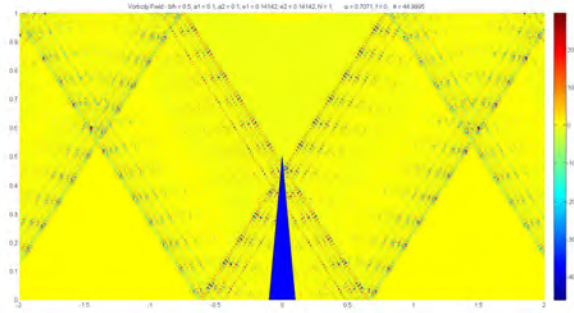
$$\phi(x, z) = \frac{1}{2} \int_0^b \gamma(z') [G(x + q(z'); z, z') + G(x - q(z'); z, z')] dz'$$

Generally speaking there are few instances when we can solve this integral equation analytically. For our model we will solve it numerically to gain an understanding of how our perturbation derived source function deviates from the basic solution for the knife edge. Once we generate the stream function we can model the internal waves by plotting the vorticity field. The vorticity  $\omega$  is defined as the curl of the velocity field,  $\omega(\mathbf{r}, t) = \nabla \times \mathbf{u}(\mathbf{r}, t)$ , which can in turn be described by the derivative of the stream function,  $(u, w) = (-\phi_z, \phi_x)$ . In the end, for the vorticity field we will be plotting the quantity:  $\omega = \frac{\partial w}{\partial x} - \frac{\partial u}{\partial z} = -(\frac{\partial^2 \phi}{\partial z^2} + \frac{\partial^2 \phi}{\partial x^2})$ .

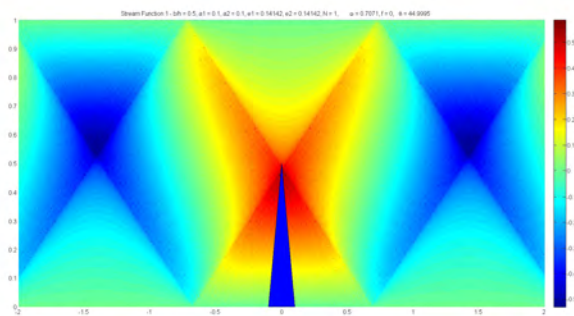
From Robinson [14] we are given the option of two different mathematical expressions for the Green's function which we can use, either the logarithmic (60) and series solution (58). Actual calculations with the two different solutions reveal differences. Although the logarithmic expression is exact, it picks up many singularities during integration which make it difficult to use in studying and modeling the stream function and vorticity field as those values tend to dominate all others. Due to this problem, we will model the stream function and vorticity field using the series expression for the Green's function, even though it has some inherent errors due to summation truncation. To justify this decision, several images will be provided of the logarithmic expression and then the series expression. For this we will have a triangular ridge with  $a_{1,2}$  and  $b = 0.5$ .



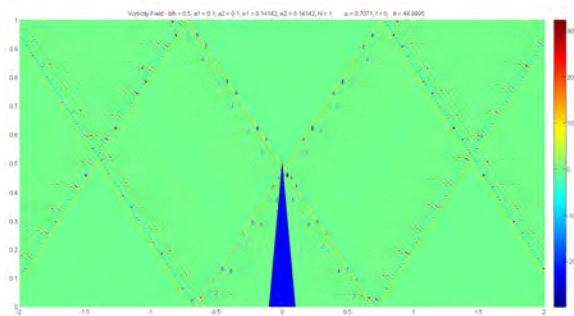
(a) Stream Function: integration interval  $N = 10$



(b) Vorticity Field: integration interval  $N = 10$



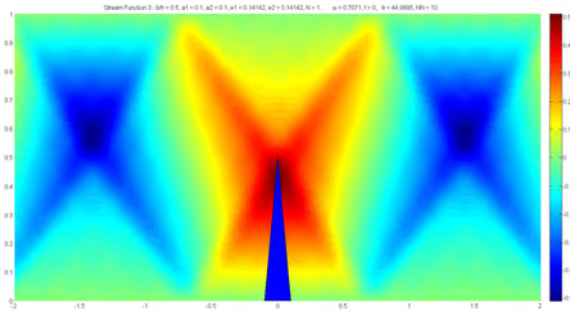
(c) Stream Function: integration interval  $N = 20$



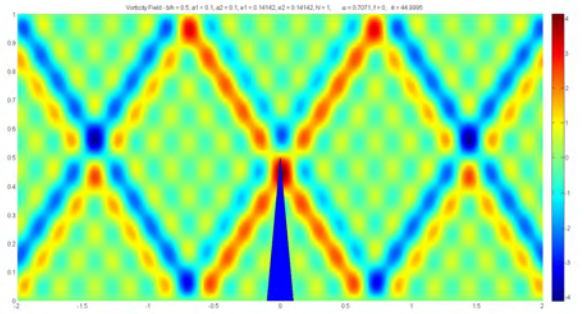
(d) Vorticity Field: integration interval  $N = 20$

Figure 5: logarithmic expression with  $x = [-2.0, 2.0]$ ,  $y = [0.0, 1.0]$ ,  $b = 0.5$ ,  $a_1 = a_2 = 0.1$

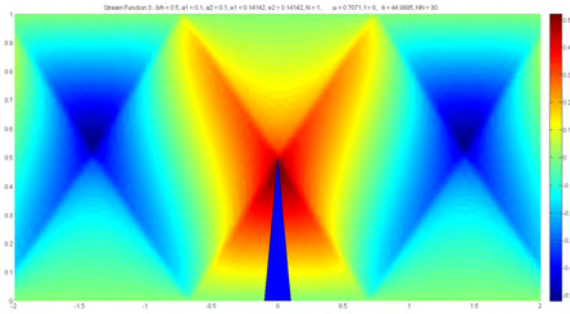
The series expression is depicted in the following figures. The series were truncated at  $n = 10, 30, 60, 100$  for each row of figures, respectively. When we reach large summation values, such as  $n = 120$ , we begin to see the similar issues as were generated by the logarithmic expression. From here on out all integration intervals will be summed over  $N = 20$  partitions, as in the second logarithmic model above, and  $n = 60$  terms. Also, the left column will always be for the Stream Function and the right column will be for the Vorticity Field.



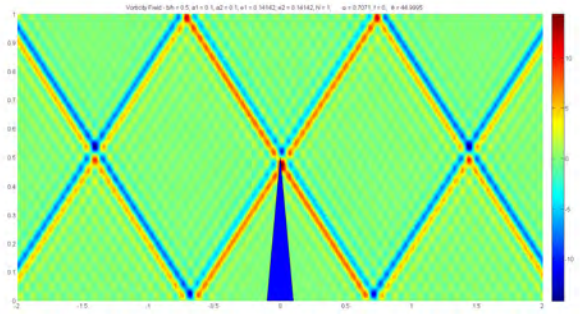
(a) summation over  $n = 10$  terms



(b) summation over  $n = 10$  terms

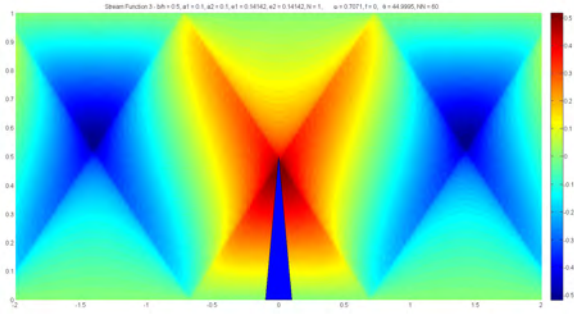


(c) summation over  $n = 30$  terms

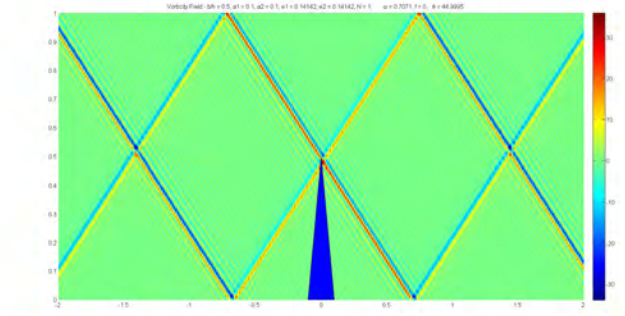


(d) summation over  $n = 30$  terms

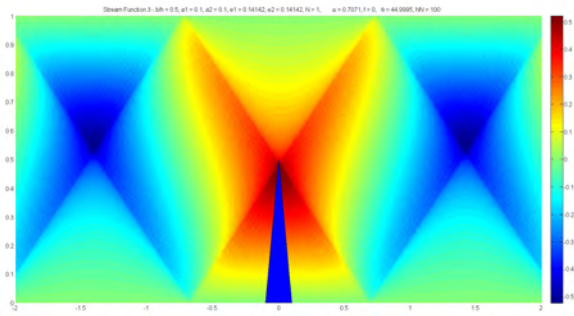
Figure 6: series expression with  $x = [-2.0, 2.0]$ ,  $y = [0.0, 1.0]$ ,  $b = 0.5$ ,  $a_1 = a_2 = 0.1$



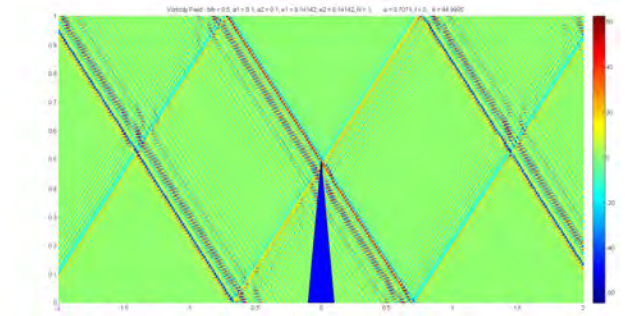
(a) summation over  $n = 60$  terms



(b) summation over  $n = 60$  terms



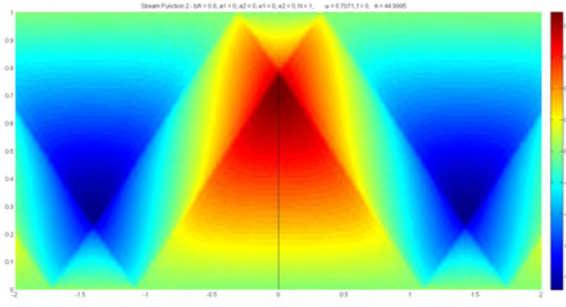
(c) summation over  $n = 120$  terms



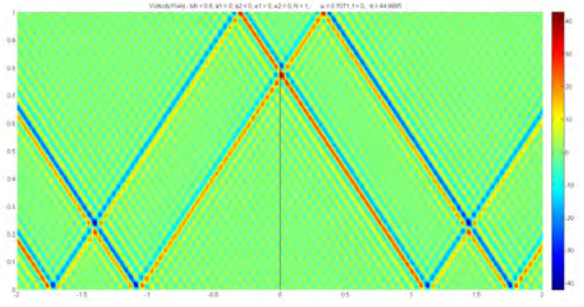
(d) summation over  $n = 120$  terms

Figure 7: series expression with  $x = [-2.0, 2.0]$ ,  $y = [0.0, 1.0]$ ,  $b = 0.5$ ,  $a_1 = a_2 = 0.1$

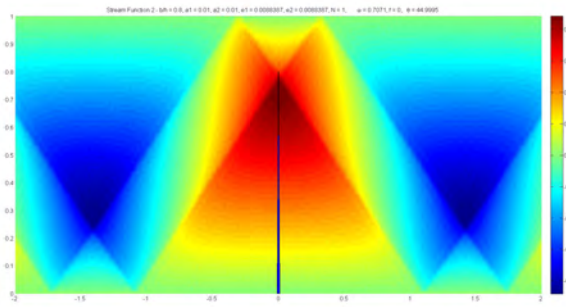
For our model we generated several surface plots of the stream function with varying properties to understand what exactly a finite width adds to the knife edge model as well as asymmetry. The first three models are of a triangle of height  $b = 0.8$  with a ray angle of  $\theta = 45^\circ$ . The first model is of a simple symmetric triangle, the same as that proposed by Pétrélis in his paper.



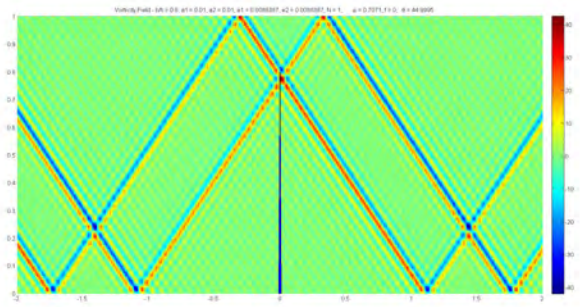
(a)  $a_1 = a_2 = 0.0$



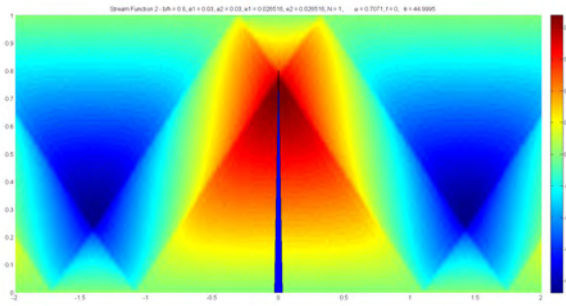
(b)  $a_1 = a_2 = 0.0$



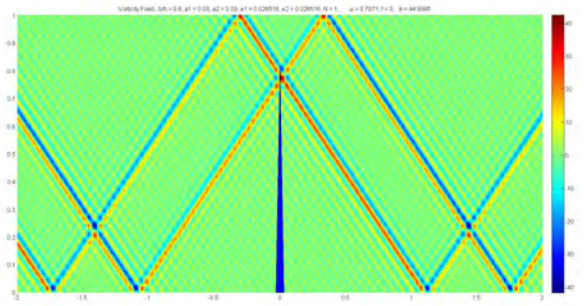
(c)  $a_1 = a_2 = 0.01$



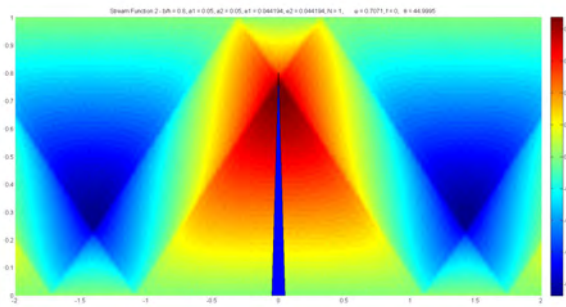
(d)  $a_1 = a_2 = 0.01$



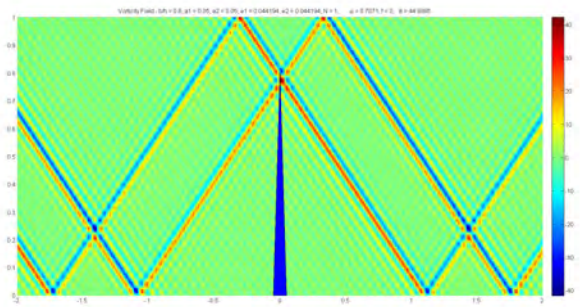
(e)  $a_1 = a_2 = 0.03$



(f)  $a_1 = a_2 = 0.03$

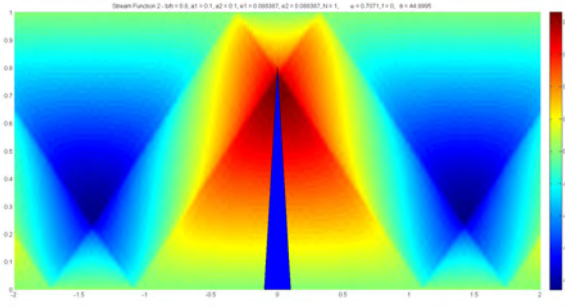


(g)  $a_1 = a_2 = 0.05$

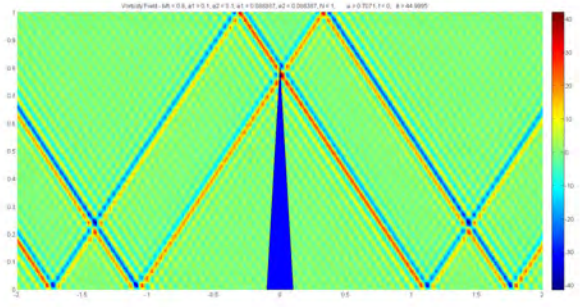


(h)  $a_1 = a_2 = 0.05$

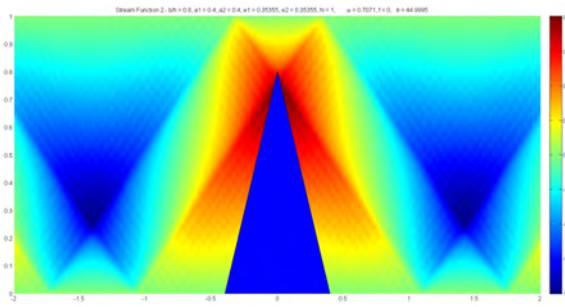
Figure 8: Model #1: Symmetric Ridge,  $x = [-2.0, 2.0]$ ,  $y = [0.0, 1.0]$ ,  $b = 0.8$ ,  $a_1 = a_2 = [0.0, 0.05]$



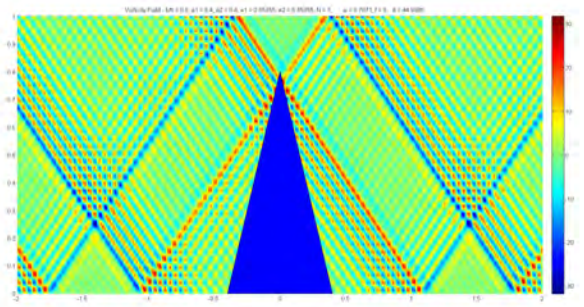
(a)  $a_1 = a_2 = 0.1$



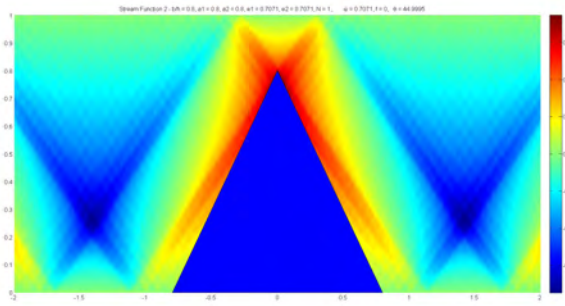
(b)  $a_1 = a_2 = 0.1$



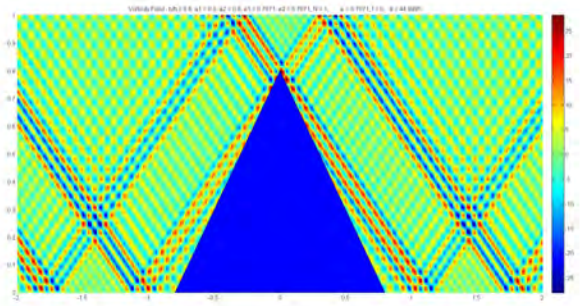
(c)  $a_1 = a_2 = 0.4$



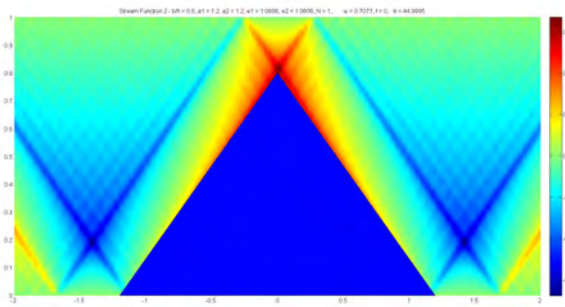
(d)  $a_1 = a_2 = 0.4$



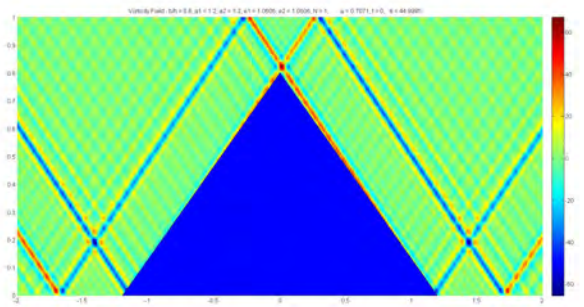
(e)  $a_1 = a_2 = 0.8$



(f)  $a_1 = a_2 = 0.8$



(g)  $a_1 = a_2 = 1.2$



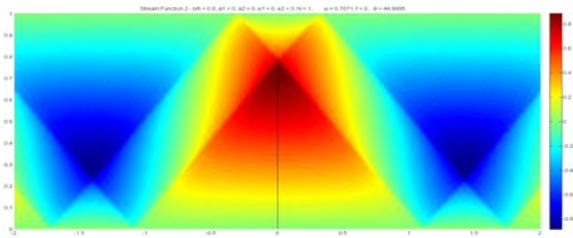
(h)  $a_1 = a_2 = 1.2$

Figure 9: Model #1: Symmetric Ridge,  $x = [-2.0, 2.0]$ ,  $y = [0.0, 1.0]$ ,  $b = 0.8$ ,  $a_1 = a_2 = [0.1, 1.2]$

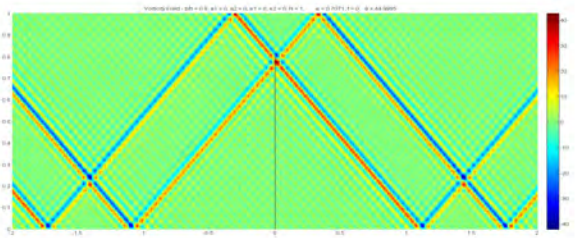
The first model gives us a simple example of perturbation theory in use. We start with keeping the perturbation factor  $\epsilon$  small, i.e. by keeping the base lengths  $a_{1,2}$  small relative to the height, but then push it further to see what sort of results we can get. When the perturbation is weak enough such that the ridge does not pass criticality, i.e. passes through the angle of the internal waves it is emitting, we can make some general conclusions. Overall, it seems that the intensity of the velocity field decreases the wider the ridge gets, which is in accordance with our plot of the conversion rate  $M$ , which described how much of the tidal energy was converted into internal waves. However, the wider the ridge gets the more we can see some faults in our approach. It is important to note that the blue image of the triangle is superimposed over the perturbation solution and so there will be noticeable discrepancies for wider ridges.

When we calculate the knife edge we see that the emission point of the internal waves is right on the top of the knife edge. However, once the ridge acquires a noticeable width we see that the strongest emission point starts to fall into the ridge, probably a result of our approximation  $b \ll h$ , which technically should not hold here since the ridge is nearly 80% of the ocean depth. Another important fault in our approach, is that it cannot handle critical and super-critical topography. This is obvious from the last image of model #1. Here the ridge has base widths larger than the height, meaning that the half-angle of the ridge exceeds  $45^\circ$ . However, our function still generates internal waves emitting downwards from the ridge tip, which is physically impossible.

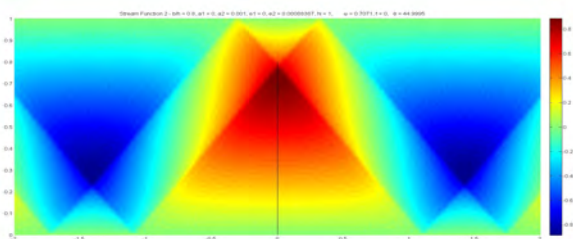
In models #2 and #3 we include an asymmetry, first with  $a_1 = 0$  and then  $a_2 = 0.1$ . The results are fairly intuitive, with the sharper ridge edge emitting stronger internal waves than the more gently sloped side. Likewise, internal waves are stronger when emitted upwards than downwards, a result that is also visible from Echeverri and Peacock's numerical analysis of asymmetric Gaussian ridges [3].



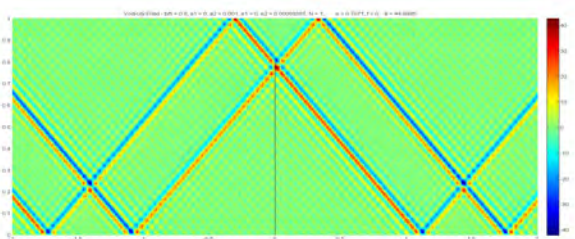
(a)  $a_2 = 0.0$



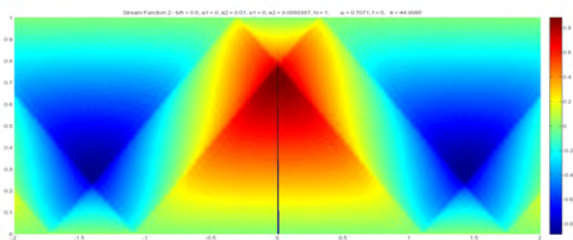
(b)  $a_2 = 0.0$



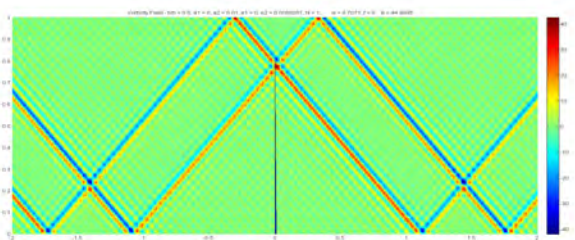
(c)  $a_2 = 0.001$



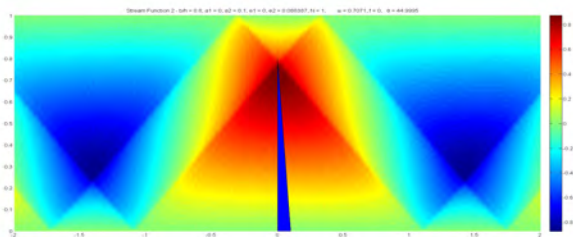
(d)  $a_2 = 0.001$



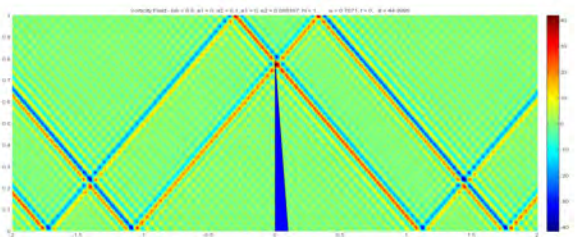
(e)  $a_2 = 0.01$



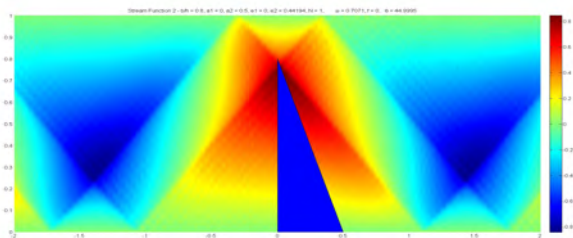
(f)  $a_2 = 0.01$



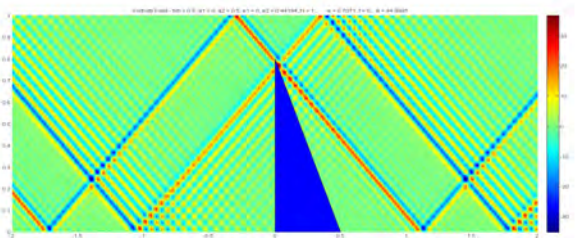
(g)  $a_2 = 0.1$



(h)  $a_2 = 0.1$

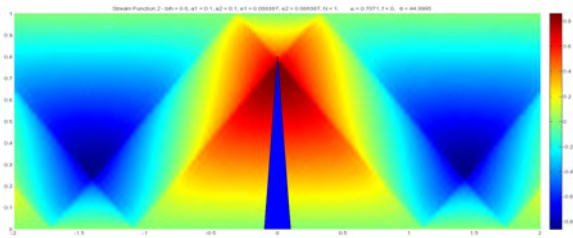


(i)  $a_2 = 0.5$

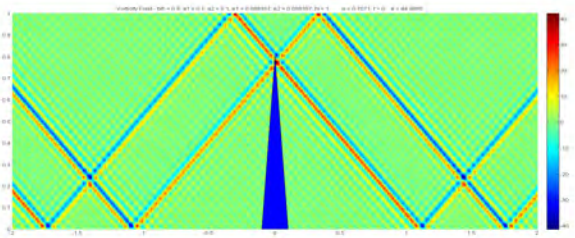


(j)  $a_2 = 0.5$

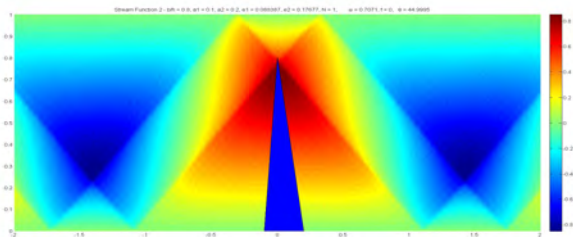
Figure 10: Model #2: Asymmetric Ridge,  $x = [-2.0, 2.0]$ ,  $y = [0.0, 1.0]$ ,  $b = 0.8$ ,  $a_1 = 0$



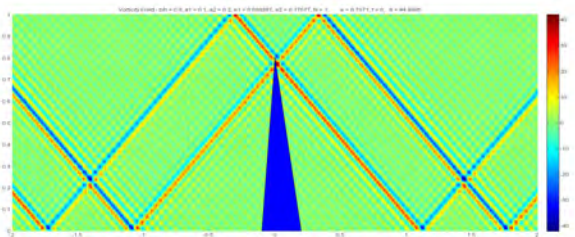
(a)  $a_2 = 0.1$



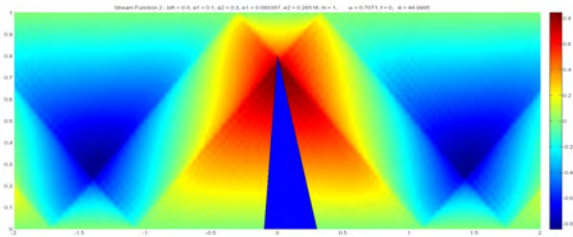
(b)  $a_2 = 0.1$



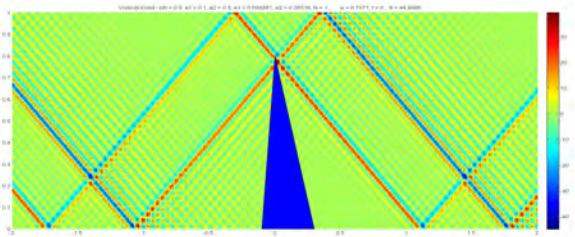
(c)  $a_2 = 0.2$



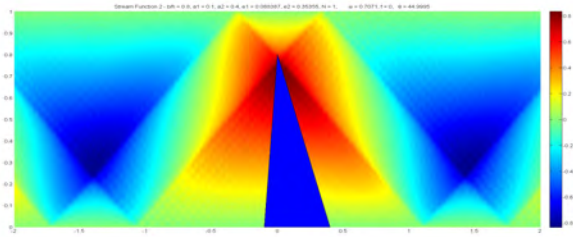
(d)  $a_2 = 0.2$



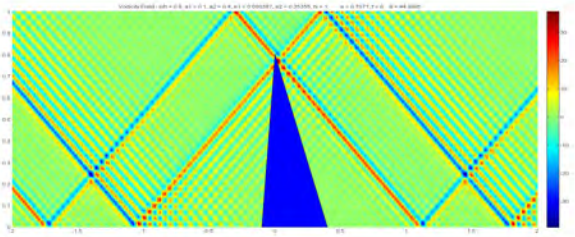
(e)  $a_2 = 0.3$



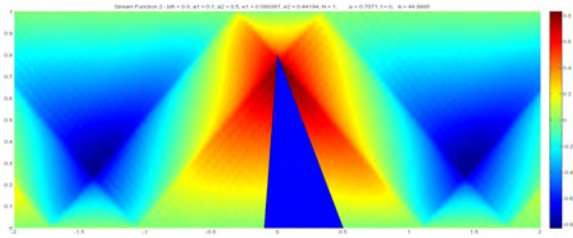
(f)  $a_2 = 0.3$



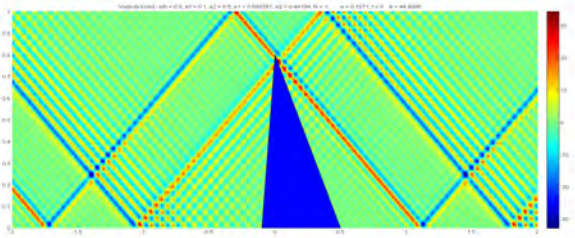
(g)  $a_2 = 0.4$



(h)  $a_2 = 0.4$



(i)  $a_2 = 0.5$

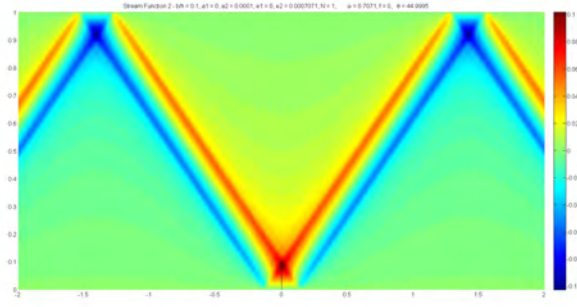


(j)  $a_2 = 0.5$

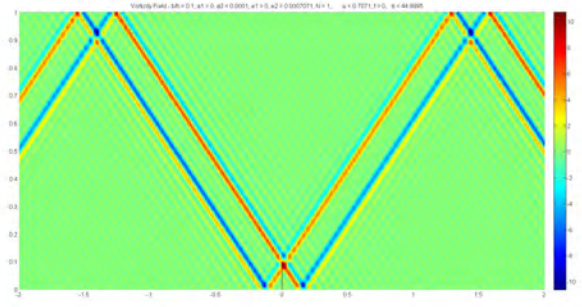
Figure 11: Model #3: Asymmetric Ridge,  $x = [-2.0, 2.0]$ ,  $y = [0.0, 1.0]$ ,  $b = 0.8$ ,  $a_1 = 0.1$

Now that we have considered tall ridges of nearly the ocean's depth in height, we will consider small ridges of height  $b = 0.1$ , more in line with the WTA approximation we we relied on to solve the finite Hilbert transform for  $\gamma_1$ . In model #4 we have an asymmetric ridge with  $a_1 = 0$ , while in model #5 we have  $a_1 = 0.001$ . In both cases we don't see as drastic of a change in the vorticity field as  $a_2$  increases compared to the tall ridge. This corresponds to our earlier analysis of the conversion rate in Figure (2). As is noticeable in the previous series of images, this model does not hold up well with the reflection of internal waves. It is able to model the trajectory of a ray, but instead of propagating an internal wave of certain intensity it merely repeats the previous emanation. It is as if the first St. Andrew's cross repeats itself periodically. Remember that we are not taking into consideration dampening or viscosity and so the intensity should stay constant under propagation.

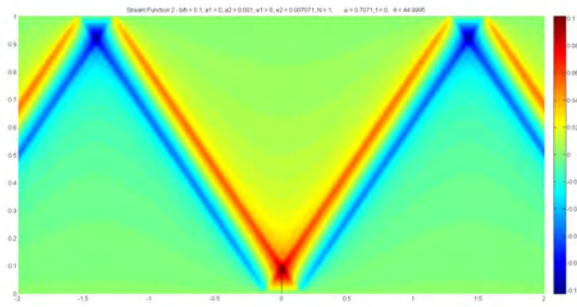
Overall the emitted internal waves do not change much in intensity until the base length approaches criticality. As the triangle approaches criticality the overall intensity of the vorticity begins to drop rapidly. Given the inability of the model to consider criticality and super-criticality, there is no sharp drop in internal wave emission once the ridge passes through the critical angle. Unlike the tall ridge, at a height of  $b = 0.1$ , the small ridge does not seem to demonstrate the same discrepancy where the emission point of the internal waves falls below the ridge tip. This is a small improvement, and can most likely be attributed to the WTA approximation  $B \ll 1$ .



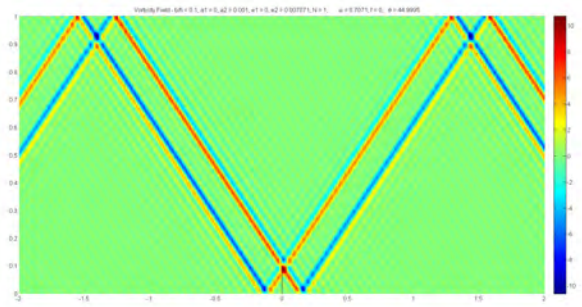
(a)  $a_2 = 0.0001$



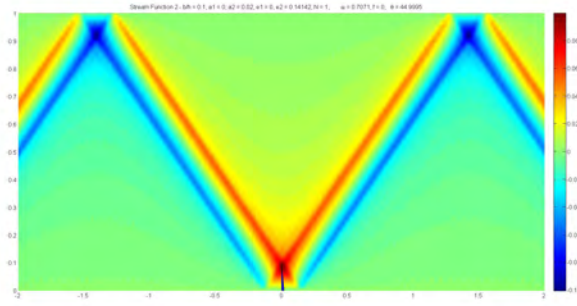
(b)  $a_2 = 0.0001$



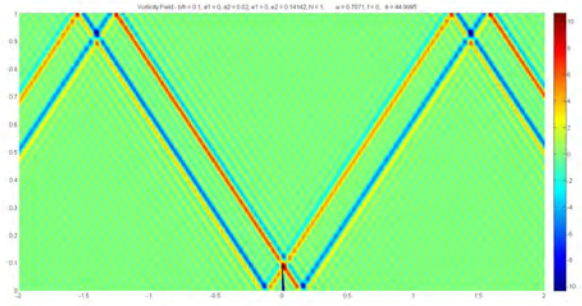
(c)  $a_2 = 0.001$



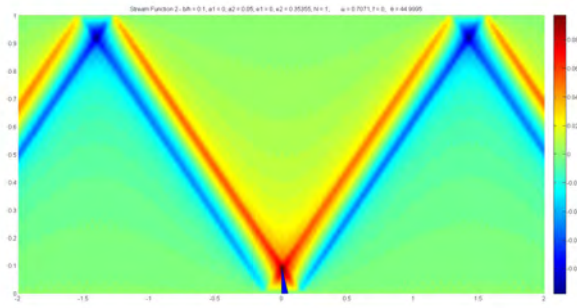
(d)  $a_2 = 0.001$



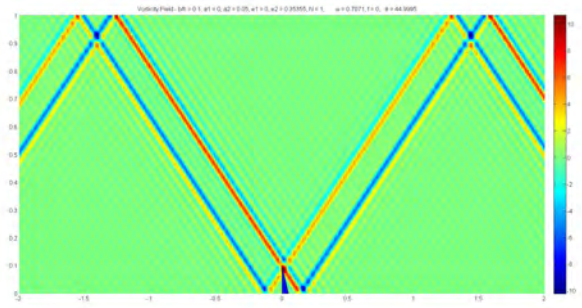
(e)  $a_2 = 0.02$



(f)  $a_2 = 0.02$

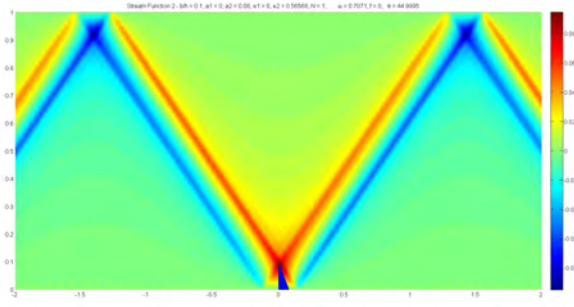


(g)  $a_2 = 0.05$

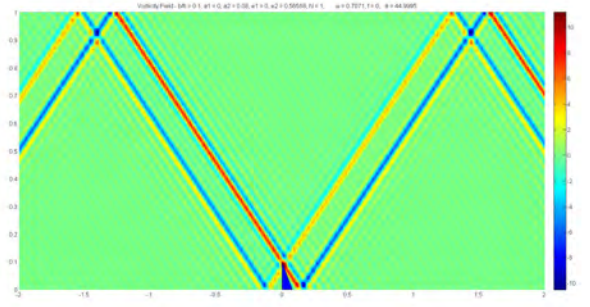


(h)  $a_2 = 0.05$

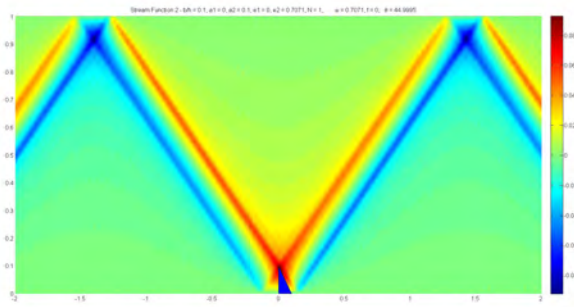
Figure 12: Model #4: Asymmetric Ridge,  $x = [-2.0, 2.0]$ ,  $y = [0.0, 1.0]$ ,  $b = 0.1$ ,  $a_1 = 0.0$



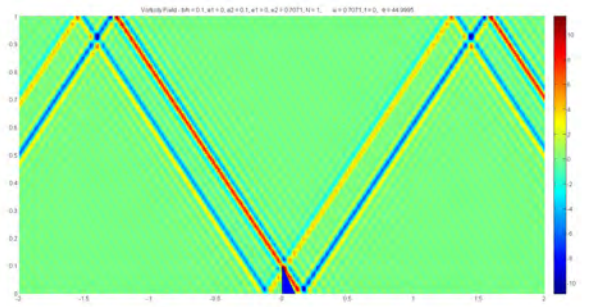
(a)  $a_2 = 0.08$



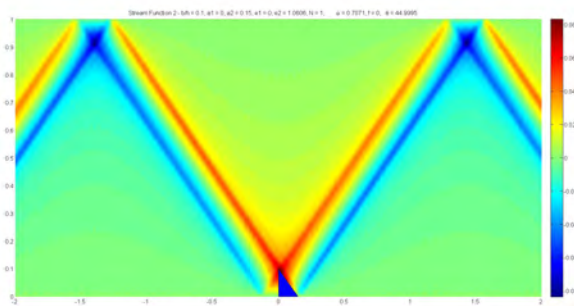
(b)  $a_2 = 0.08$



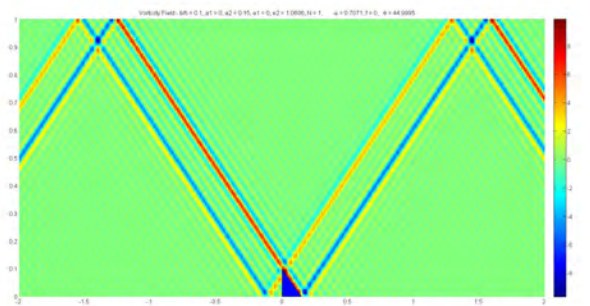
(c)  $a_2 = 0.1$



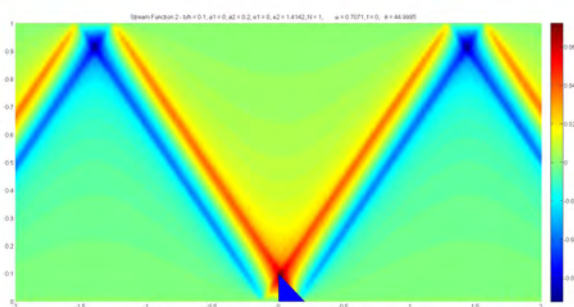
(d)  $a_2 = 0.1$



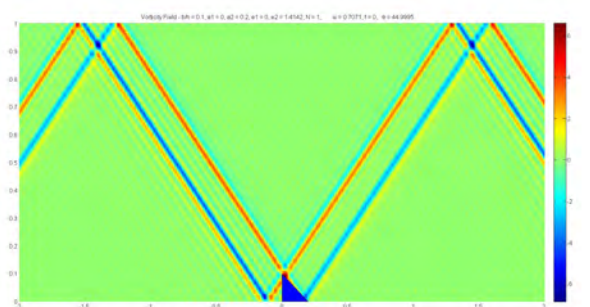
(e)  $a_2 = 0.15$



(f)  $a_2 = 0.15$

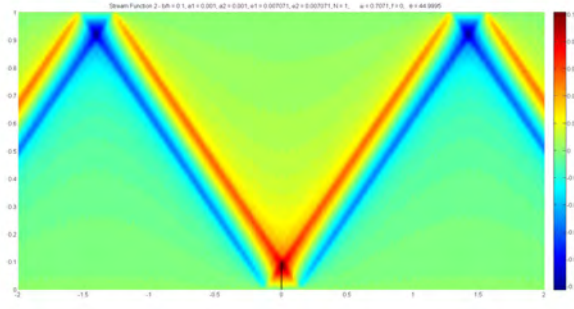


(g)  $a_2 = 0.2$

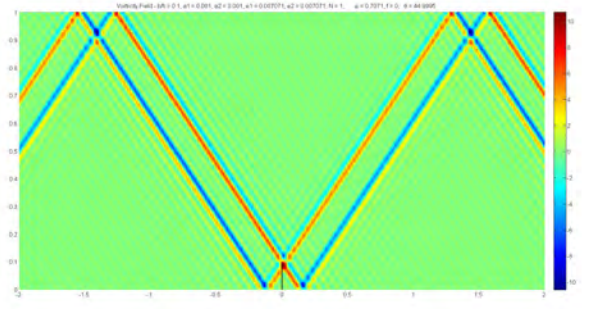


(h)  $a_2 = 0.2$

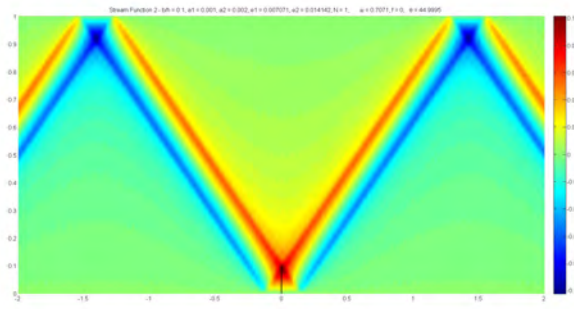
Figure 13: Model #4: Asymmetric Ridge,  $x = [-2.0, 2.0]$ ,  $y = [0.0, 1.0]$ ,  $b = 0.1$ ,  $a_1 = 0.0$



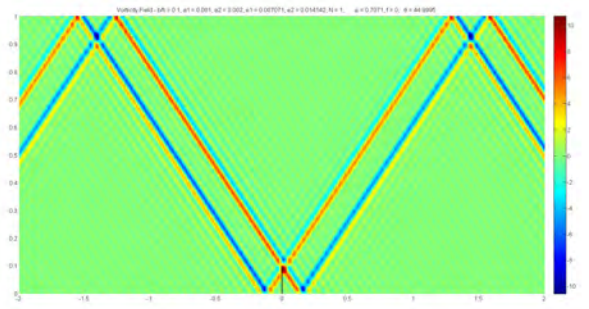
(a)  $a_2 = 0.001$



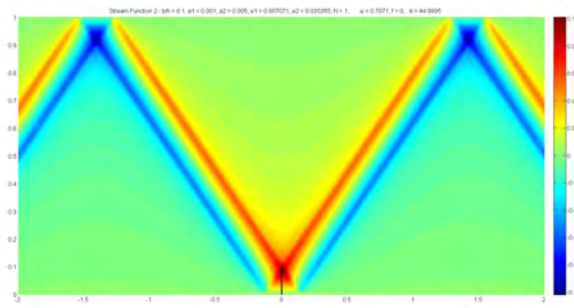
(b)  $a_2 = 0.001$



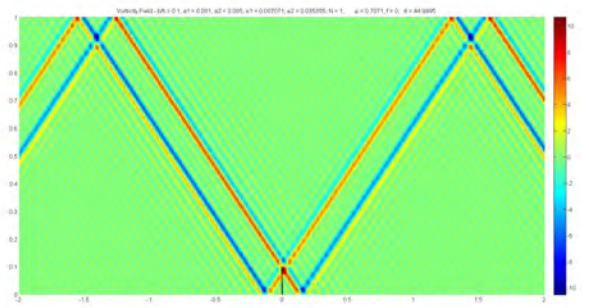
(c)  $a_2 = 0.002$



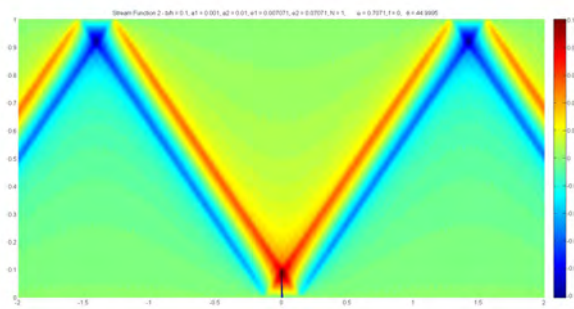
(d)  $a_2 = 0.002$



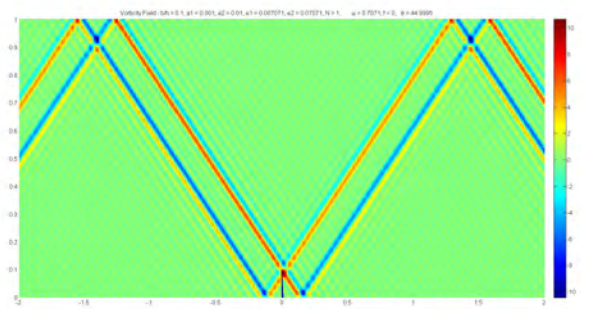
(e)  $a_2 = 0.005$



(f)  $a_2 = 0.005$



(g)  $a_2 = 0.01$



(h)  $a_2 = 0.01$

Figure 14: Model #5: Asymmetric Ridge,  $x = [-2.0, 2.0]$ ,  $y = [0.0, 1.0]$ ,  $b = 0.1$ ,  $a_1 = 0.001$



To get a better understanding of the behavior of internal waves, we will now focus in on the ridge tip itself to see how internal waves behave at the emission point. We do this for ridges of both heights  $b = 0.8$  and  $b = 0.1$ . Once again, in order to avoid singularities we used the series summation to model the waves instead of the logarithmic expression. However, we are now focused on a smaller field of observation (here we are looking at the region  $x = [-0.1, 0.1]$  and  $y = [0.7, 0.9]$ ). In previous images we were looking at  $x = [-2, 2]$  and  $y = [0, 1]$ ). We increased the value of  $n$  for the sum from 30 to 100 in order to visualize a reasonable convergence. The tall ridge is interesting in that the internal waves emitted seem to come out fractured, with beams of alternating vorticity propagating from the tip of the ridge.

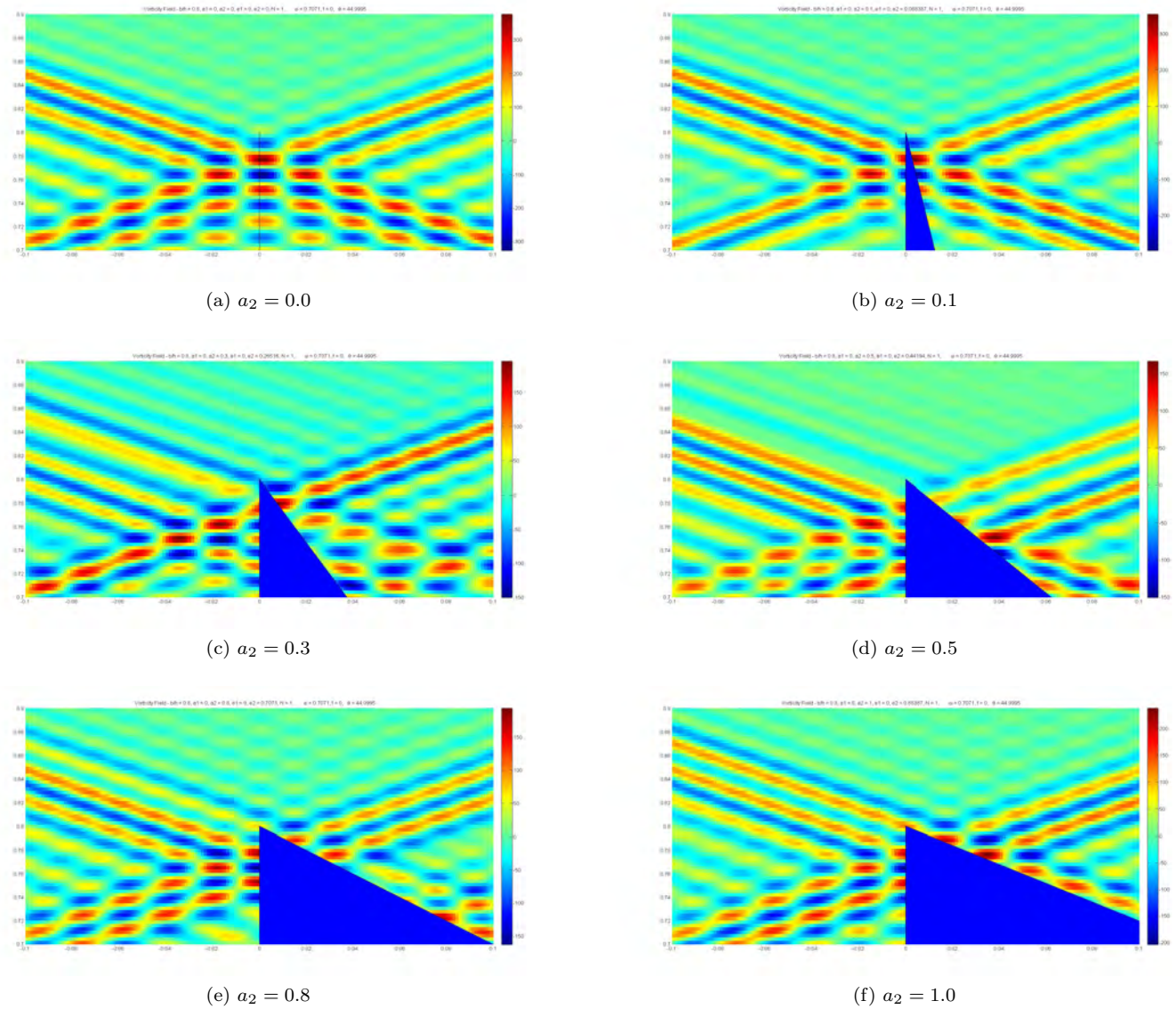
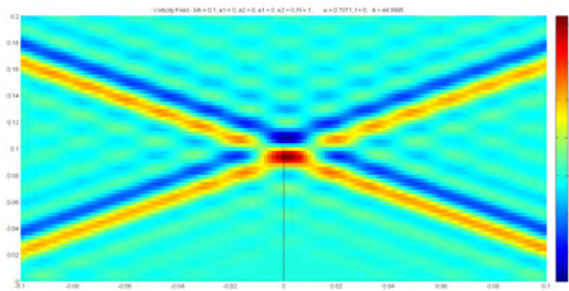
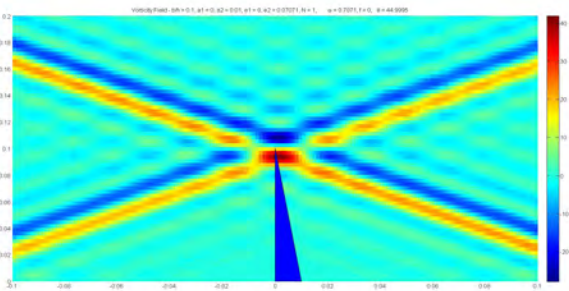


Figure 16: Model #6: Asymmetric Ridge,  $x = [-0.1, 0.1]$ ,  $y = [0.7, 0.9]$ ,  $b = 0.8$ ,  $a_1 = 0.0$ ,  $a_2 = [0.0, 1.0]$

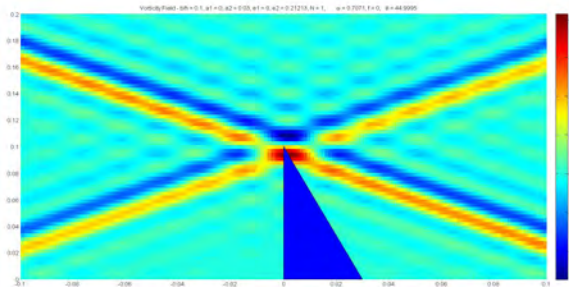
Unlike the case for the tall ridge, the short ridge of height  $b = 0.1$  does not demonstrate the same fracturing of the beam. In fact it comes out as merely two parallel beams of opposite vorticities propagating away from the ridge tip. Another thing to note, we have to truncate the series much later in order to observe anything sensible at all, truncating the series at the  $100^{th}$  term as opposed to the  $30^{th}$ , in both this system and the last. As in the previous case, we are looking at a much smaller field of observation, the region  $x = [-0.1, 0.1]$  and  $y = [0, 0.2]$ . It seems overall that the beam is stronger in respect to positive vorticity, but this might just be an artifact of the truncated summation. Likewise, it seems like there is evidence of the singularity near the ridge tip, where the vorticity is most intense.



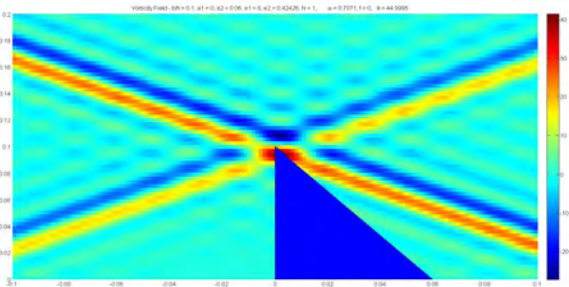
(a)  $a_2 = 0.0$



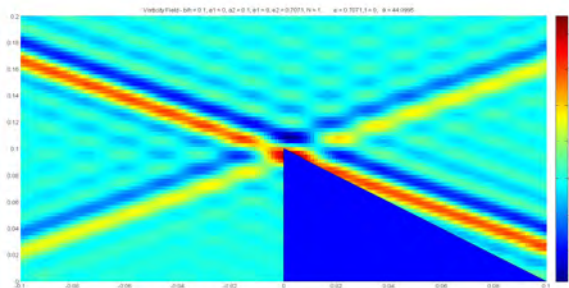
(b)  $a_2 = 0.01$



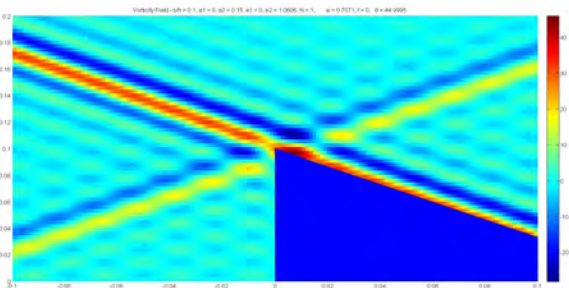
(c)  $a_2 = 0.03$



(d)  $a_2 = 0.06$



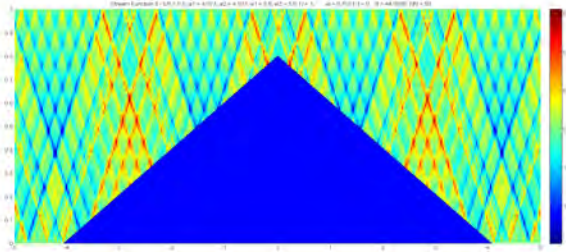
(e)  $a_2 = 0.1$



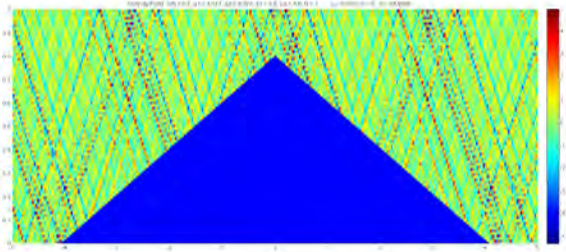
(f)  $a_2 = 0.15$

Figure 17: Model #7: Asymmetric Ridge,  $x = [-0.1, 0.1]$ ,  $y = [0.0, 0.2]$ ,  $b = 0.1$ ,  $a_1 = 0.0$ ,  $a_2 = [0.0, 0.15]$

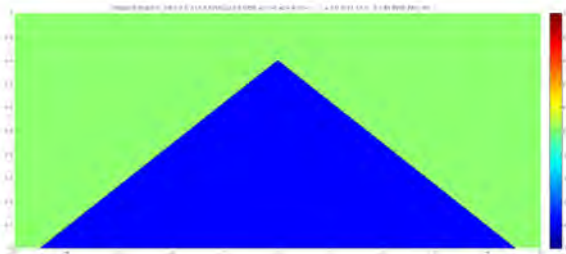
Given our mathematical description of the system, we know that somewhere in the range of the perturbation term  $\epsilon$  there is a value that will cause the source function to fall to zero, theoretically causing the stream function and vorticity field to vanish. This can be calculated analytically by observing in equation (82) that when  $\epsilon = 4$  the perturbed source function falls to zero. This means that for a ridge of height  $b = 0.8$ , with a half base length of  $a_{1,2} = 4 * b * \mu = 4.5255$  we should get the null solution. Denoting the null solution as  $a_0$ , we model the system for three baselengths of  $a_{1,2}$  equal to  $0.9a_0$ ,  $1.0a_0$ , and  $1.1a_0$ . As seen in Figure (18), just as we predicted, at a certain half base length the perturbed vorticity field vanishes. However given that this base length is quite super critical, inclusion of higher order terms is required to get a more accurate picture of such a system.



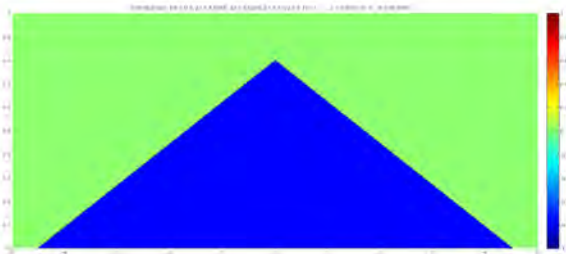
(a)  $a_{1,2} = 0.9a_0$



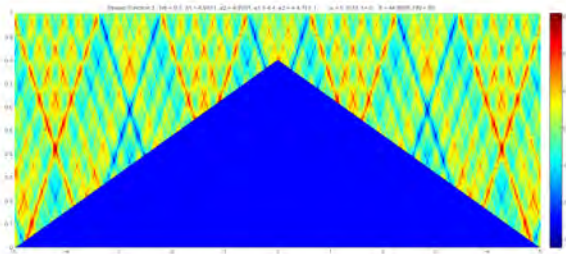
(b)  $a_{1,2} = 0.9a_0$



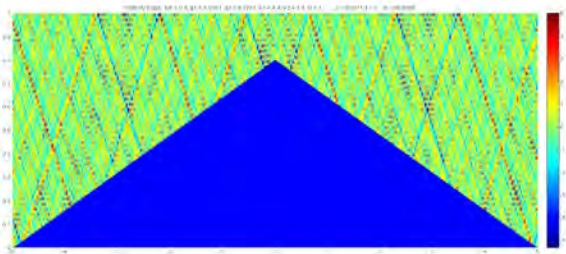
(c)  $a_{1,2} = 1.0a_0$



(d)  $a_{1,2} = 1.0a_0$



(e)  $a_{1,2} = 1.1a_0$



(f)  $a_{1,2} = 1.1a_0$

Figure 18: Model #8: Symmetric Ridge - Null Solution,  $x = [-5.0, 5.0]$ ,  $y = [0.0, 1.0]$ ,  $b = 0.8$

Another system we can attempt to model is that of a steep cliff. This we will do simply by saying that  $a_1 = 0$  and then make  $a_2$  some very large number, for example 1000. We presented results of this modeled below for a ridge of height  $b = 0.5$ . It has already been established that our ridge cannot model a system for which the half angle of the ridge is greater than the critical angle. Nevertheless, it may be interesting to see how our numerics behave. As is evident there is already some discrepancy as internal waves are not emitted from the edge of the cliff. Likewise, the emitted waves are the same on both sides of the cliff, while in reality you would have large internal waves propagating to the left and smaller, rapidly reflecting waves propagating to the right. A study by St. Laurent [15] more successfully models this system by matching the velocity fields at the the interface at  $x = 0$ , but his technique is beyond the scope of this paper.

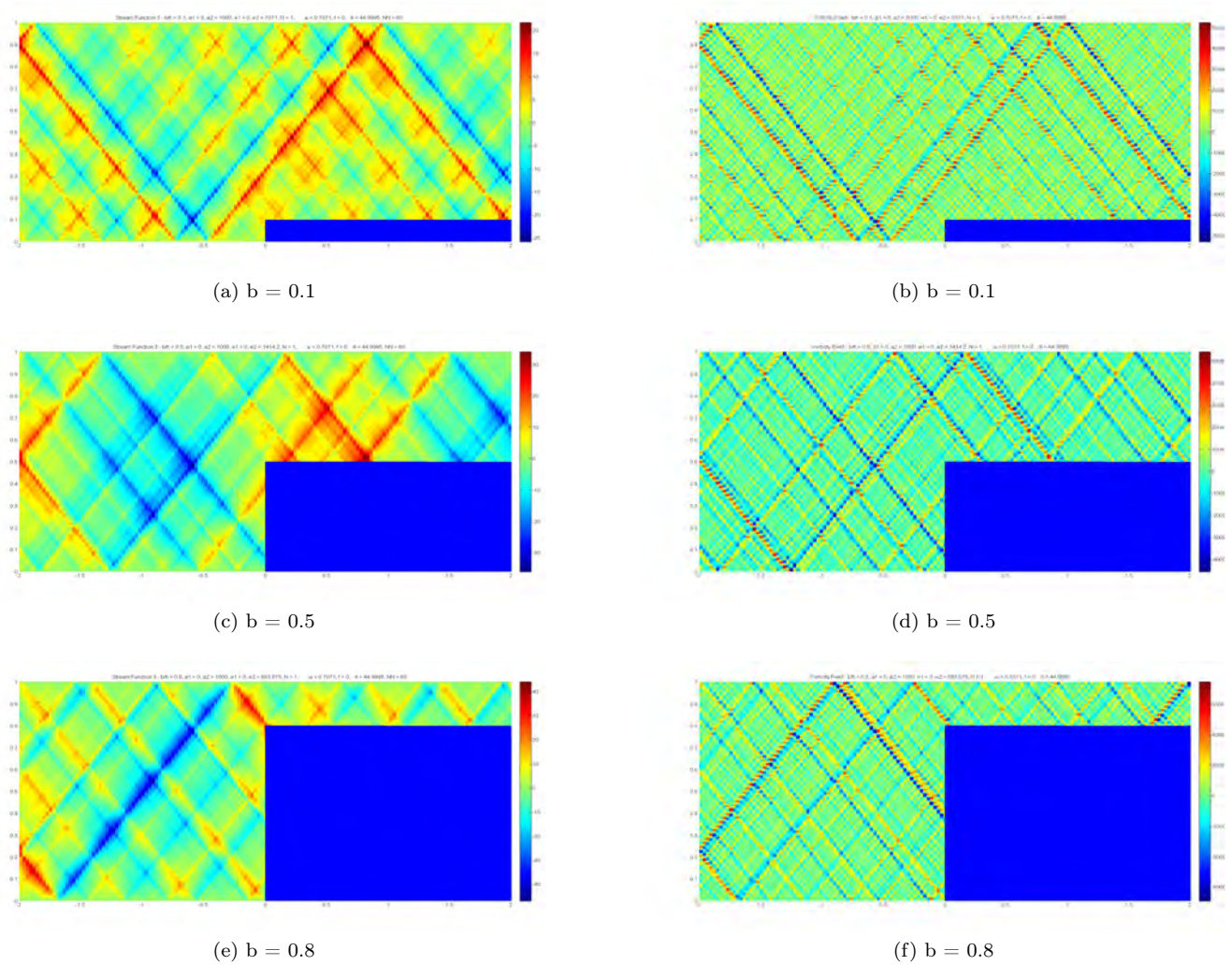


Figure 19: Model #9: Asymmetric Ridge - Cliff,  $x = [-2.0, 2.0]$ ,  $y = [0.0, 1.0]$ ,  $a_1 = 0$ ,  $a_2 = 1000$

## 5 Conclusion

The application of perturbation theory to our system of a thin, triangular ridge has demonstrated both the usefulness of this approach as well as its limitations. In some respects the approach we took is almost antiquated given the power of numerical methods to model and calculate different systems. Such approaches as those of Echeverri and Peacock and St. Laurent are more powerful and more accurate. However, an analytical description of a system can often be more informative, faster, and give us certain predictive powers that numerics cannot. Despite the limitations of our approach we were able to make several conclusions.

Using the knife edge solution as originally produced by Robinson [14], Pétrélis [13], and Smith and Young [8], we were able to carry further study of a thin ridge by adding a small thickness to it. This was done by using perturbation theory to expand on the Green's function solution and the source function  $\gamma$  for a first order correction to the knife edge. Our results were more or less intuitive, that by adding a small thickness to the ridge we could modify and lessen the strength of emitted internal waves. Likewise, adding asymmetry to our system was also similarly intuitive, with the sharper slopes emitting stronger internal waves. However, our approach clearly began to demonstrate problems as we approached the critical angle for the internal wave. Our model was unable to correctly model the system from that point on, as downwards propagating waves were still emitted even though the slope of the ridge made that a physical impossibility. We did demonstrate, however, that for when the perturbation is small, we can effectively model the effects of asymmetry and non-infinitesimal topography analytically.

Another object we were able to study was the conversion rate  $M$ . Expanding the conversion rate in the perturbation term  $\epsilon$  so that we get  $M = M_{knife}(B) + \epsilon^2 M_2(B)$ , we were able to model the effects of ridge height and thickness on the conversion of tidal energy into internal waves. In both cases, when we increased the height or thickness of the ridge the conversion rate fell, suggesting that the knife edge is the strongest generator of internal waves for varying topography. This contradicts several previous studies that claimed that the critical angle is the most powerful system for the generation of internal waves. In addition to this study, we also found a critical base length for which the vorticity field vanishes and goes to zero.

Overall this thesis study has proven fruitful not only as a physical investigation but also as a mathematical study, presenting various challenging problems and using advanced mathematical techniques to solve those problems. In addition to perturbation theory, we also used special mathematical constructs such as the Green's function, WKB approximation, integral equation, and finite Hilbert transform to generate a solution for the triangular ridge. Mathematics is the language of science and the more we are able to master it the more we are able to understand the physical world around us.

## References

- [1] Balmforth, P.G., G.R. Ierley, and W.R. Young, "Tidal conversion by subcritical topography." *J. Phys. Oceanogr.* 32, 2900-2914 (2002)
- [2] Bell Jr., T.H., "Topographically generated waves in the open ocean." *J. of Geop. Res.* 90, 3, 320 (1975)
- [3] Echeverri, P., and T. Peacock, "Internal tide generation by arbitrary two-dimensional topography." *J. Fluid Mech.* 659, 247-266 (2010)
- [4] Khatiwala, S., "Generation of internal tides in the coean." *Deep-Sea Res. I*, 50 (2003)
- [5] Kundu, P.K., I.M. Cohen, and D.R. Rowling, "Fluid Mechanics." Waltham: Elsevier Inc., 2012
- [6] Lamb, Sir H., "Hydrodynamics." Cambridge: Cambridge University Press, 1995
- [7] Llewellyn Smith, S.G., and W.R. Young, "Conversion of the barotropic tide." *J. Phys. Oceanogr.* 32, 1554-1566 (2002)
- [8] Llewellyn Smith, S.G., and W.R. Young, "Tidal conversion at a very steep ridge." *J. Fluid Mech.* 495, 175-191 (2003)
- [9] Matthews, J., and R.L. Walker, "Mathmematical Methods of Physics." Redwood City: Addison-Wesley Publishing Company, 2nd ed., 1970
- [10] Nycander, J., "Tidal generation of internal waves from a periodic array of steep ridges." *J. Fluid Mech.* 567, 415-432 (2006)
- [11] Pedlosky, J., "Geophysical Fluid Dynamics." New York: Springer, 1987
- [12] Pedlosky, J., "Waves in the Ocean and Atmosphere: Introduction to Wave Dynamics." New York: Springer, 2003
- [13] Pétrélis, F., S. Llewellyn Smith, and W.R. Young, "Tidal conversion at a submarine ridge." *J. Phys. Oceanogr.* 36, 1053 (2006)
- [14] Robinson, R.M., "The effects of a barrier on internal waves." *Deep-Sea Res.* 16, 421-429 (1969)
- [15] St. Laurent, L., S. Stringer, C.J.R. Garrett, and D. Perrault-Joncas, "The generation of internal tides at abrupt topography." *Deep-Sea Res. I*, 50, 987-1003 (2003)
- [16] Tabaei, A., and T.R. Akylas, "Nonlinear internal gravity waves beams." *J. Fluid Mech.* 482, 141-161 (2003)
- [17] Tabaei, A., T.R. Akylas, and K.G. Lamb, "Nonlinear effects in reflecting and colliding internal wave beams." *J. Fluid Mech.* 526, 217-243 (2005)